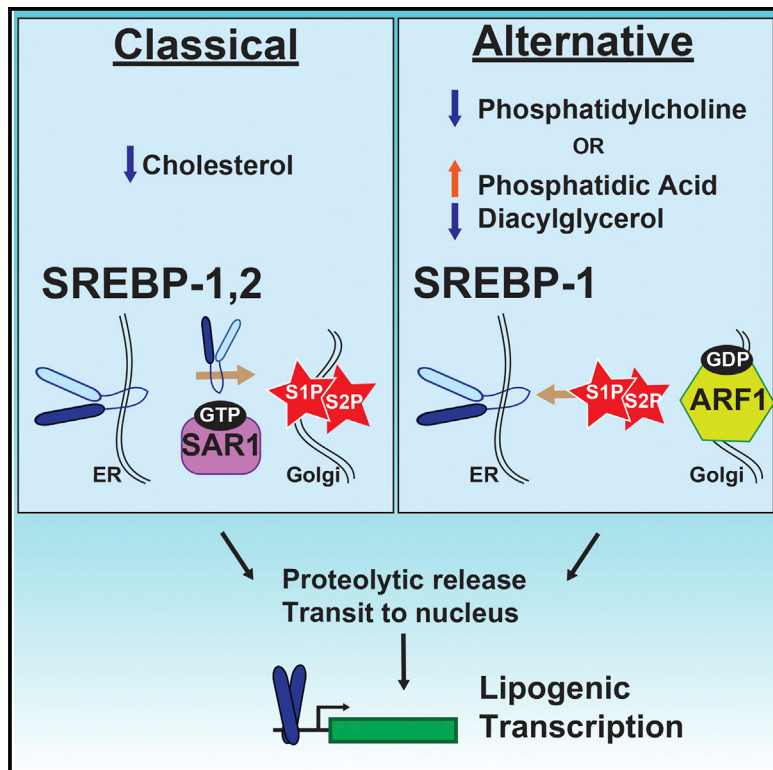


Cholesterol-Independent SREBP-1 Maturation Is Linked to ARF1 Inactivation

Graphical Abstract



Authors

Lorissa J. Smulan, Wei Ding,
Elizaveta Freinkman, Sharvari Guja,
Yvonne J.K. Edwards, Amy K. Walker

Correspondence

amy.walker@umassmed.edu

In Brief

SREBP transcription factors may be proteolytically activated in response to low cholesterol or by low phosphatidylcholine (PC) by distinct mechanisms. Smulan et al. find that SREBP-1 processing in low PC is linked to changes in phosphatidic acid, diacylglycerol, or PC in microsomal membranes leading to decreases in active GTP-bound ARF1.

Highlights

- A *C. elegans* screen finds *lpn-1* and *arf-1.2* as necessary for low-PC SREBP-1 activation
- Depletion of mammalian *LPIN1* and *ARF1* activates SREBP-1 and rescues low-PC effects
- Levels of active ARF fall when PC synthesis is blocked or *LPIN1* is depleted
- Blocking PC synthesis or *LPIN1* siRNA decreases GBF1 association with microsomes

Cholesterol-Independent SREBP-1 Maturation Is Linked to ARF1 Inactivation

Lorissa J. Smulan,¹ Wei Ding,¹ Elizaveta Freinkman,² Sharvari Gujja,¹ Yvonne J.K. Edwards,¹ and Amy K. Walker^{1,*}¹Program in Molecular Medicine, UMASS Medical School, 373 Plantation Street, Worcester, MA 01605, USA²Metabolite Profiling Facility, Whitehead Institute for Biomedical Research, 9 Cambridge Center, Cambridge, MA 02142, USA

*Correspondence: amy.walker@umassmed.edu

<http://dx.doi.org/10.1016/j.celrep.2016.05.086>

SUMMARY

Lipogenesis requires coordinated expression of genes for fatty acid, phospholipid, and triglyceride synthesis. Transcription factors, such as SREBP-1 (Sterol regulatory element binding protein), may be activated in response to feedback mechanisms linking gene activation to levels of metabolites in the pathways. SREBPs can be regulated in response to membrane cholesterol and we also found that low levels of phosphatidylcholine (a methylated phospholipid) led to SBP-1/SREBP-1 maturation in *C. elegans* or mammalian models. To identify additional regulatory components, we performed a targeted RNAi screen in *C. elegans*, finding that both *lpn-1/Lipin 1* (which converts phosphatidic acid to diacylglycerol) and *arf-1.2/ARF1* (a GTPase regulating Golgi function) were important for low-PC activation of SBP-1/SREBP-1. Mechanistically linking the major hits of our screen, we find that limiting PC synthesis or *LPN1* knockdown in mammalian cells reduces the levels of active GTP-bound ARF1. Thus, changes in distinct lipid ratios may converge on ARF1 to increase SBP-1/SREBP-1 activity.

INTRODUCTION

Metabolic gene regulation is often connected to products or substrates in the pathway. In some cases, such as low-cholesterol stimulated maturation of SREBP (sterol regulatory element binding protein) transcription factors, mechanisms have been described in detail. SREBPs reside in the endoplasmic reticulum (ER) as membrane intrinsic, inactive precursors (Osborne and Espenashade, 2009). Drops in intra-membrane cholesterol promote transport of SREBP to the Golgi (Goldstein et al., 2006) where proteases release the transcriptionally active portion (Brown and Goldstein, 1997). SREBPs regulate genes required for fatty acid, TAG (triglyceride), PC (phosphatidylcholine), and cholesterol synthesis (Horton et al., 2002); therefore, it is not surprising that control of SREBP activity is complex and responds to a variety of metabolic signals. SREBP-2 is tightly linked to cholesterol synthesis, whereas the SREBP-1a/c isoforms have

broader roles (Horton, 2002). Using *C. elegans* and mammalian models, we previously found that low levels of SAM acted through PC to induce cholesterol-independent SREBP-1 processing (Walker et al., 2011). Instead of depending on COP II transit to the ER, low PC was associated with dissolution of Golgi markers, suggesting SREBP-activating proteases may cleave ER bound SREBP-1, as in Brefeldin-A mediated activation (DeBose-Boyd et al., 1999). However, regulatory factors linking PC to these processes were unclear.

To identify additional factors in this pathway, we performed a *C. elegans* RNAi screen using the SBP-1/SREBP-1 responsive reporter. Our genetic approach identified *lpn-1/LPIN1* and *arf-1.2/ARF1*, suggesting that, like cholesterol-dependent regulation of SREBP-2, low-PC effects on SREBP-1 are linked to effects of membrane lipids on intracellular transport; however, in this case, intermediates in the TAG/PC synthesis pathway, such as PA and DAG, may affect Golgi to ER COP I function.

RESULTS

Targeted RNAi Screen to Reveal Low-PC Modulators of SBP-1

To identify components in low-PC activation of SBP-1/SREBP-1, we performed a targeted RNAi screen comparing activation of a SBP-1-dependent reporter, *pfat-7::GFP*, in wild-type and low-PC conditions. *fat-7* encodes a stearoyl-CoA desaturase (SCD) regulated by SBP-1 (Yang et al., 2006). Depletion of PC synthesis enzymes (*sams-1*, *pmt-1*, *cept-1*, *pcyt-1*), stimulates SBP-1 and *fat-7* levels increase (Walker et al., 2011) (Figure 1A). We focused on metabolic pathways producing or utilizing PC, genes involved in lipid-based signaling, and a subset of genes linked to COP I or II transport. Next, we selected an RNAi sublibrary from the ORFeome collection (Rual et al., 2004), the Ahringer library (Kamath et al., 2003), or constructed RNAi targeting vectors (Table S1). We screened for candidates satisfying two criteria: first, necessary for *pfat-7::GFP* induction in low-PC *sams-1(lf)* animals, and second, sufficient to activate *pfat-7::GFP* in wild-type phospholipid levels (Figure 1B).

We screened four library replicates and divided candidates into four classes according to GFP expression and genotype (Figure 1B; Table S1). Class 1 or class 2 genes limited or increased *pfat-7::GFP* expression and comprised 49 (23%) or 10 (5%) of clones screened. Candidate class 3 genes were associated with decreases in *sams-1(lf)*; *pfat-7::GFP* (68 genes), and



CrossMark

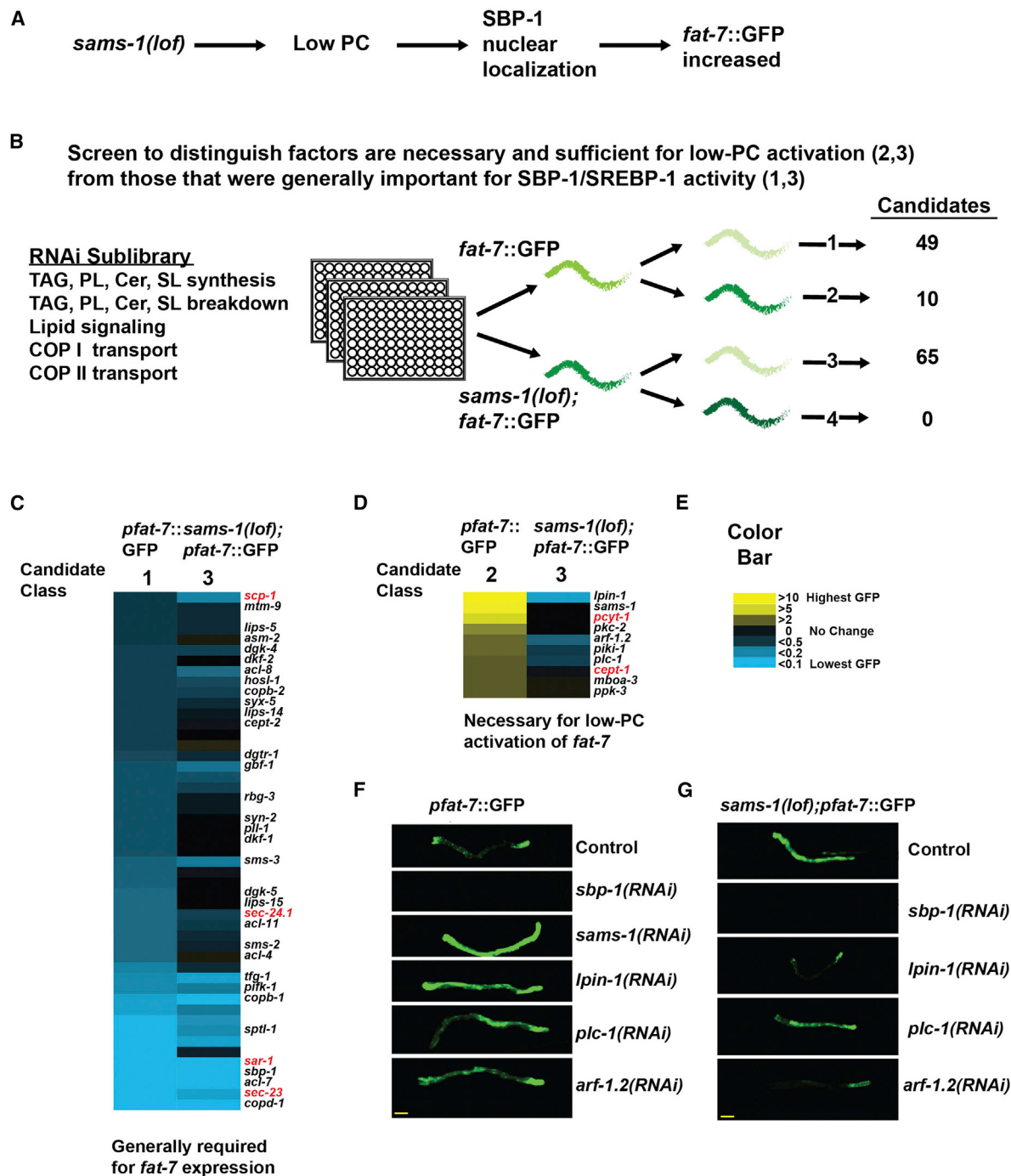


Figure 1. Targeted RNAi Screen to Identify Modulators of SBP-1/SREBP-1 Activation in Low PC Conditions in *C. elegans*

(A) Schematic representation of low-phosphatidylcholine (PC)-based SBP-1/SREBP-1 activation in *C. elegans*.

(B) Schematic representation of RNAi screen designed to distinguish factors necessary and sufficient for low-PC based SBP-1 activation (classes 2 and 3) from those generally required for SBP-1 function (classes 1 and 3).

(C) Heatmap showing genes which downregulate fat-7 expression in both pfat-7::GFP and sams-1(*lof*);pfat-7::GFP animals.

(D) Heatmap showing genes increasing fat-7 expression in pfat-7::GFP animals, while reducing GFP expression in sams-1(*lof*);pfat-7::GFP animals.

(E) Color bar representing averaged GFP scores represented by yellow (high) and by blue (low).

(F and G) Epifluorescence imaging showing RNAi of class 2/3 candidates in pfat-7::GFP (F) or sams-1(*lof*);pfat-7::GFP (G) in young adult *C. elegans*. Scale bar, 75 μm. See also Table S1 and Figure S1.

there were no genes that increased *pfat-7::GFP* in *sams-1(lf)* animals (class 4). Class 1 and class 3 genes are predicted to be generally important for SBP-1 function and indeed include many regulators of classical SREBP-1 processing such as *scp-1* (SCAP, SREBP cleavage-activating protein) and the COP II components such as *sec-23*, *sec-24.1*, and *sar-1* (Figure 1C, red lettering). As in our previous data, PC synthesis genes (*pcyt-1* and *cept-1*) (Figure 1D, red labeling) fell into class 2 (Walker et al., 2011). Genes necessary for low-PC processing and sufficient to activate SBP-1 in normal PC (Figure 1D, red lettering) were predicted to lie in the intersection of candidate classes 2 and 3. The GTPase *arf-1.2* was present in this category, as well a phospholipase C ortholog. However, the PA phosphatase *lpin-1* (Reue, 2007) showed the most striking increase in *pfat-7::GFP* combined with decrease in *sams-1(lf);pfat-7::GFP* (Figures 1D–1G; Table S1).

Next, we used qRT-PCR to determine expression of *gfp*, endogenous *fat-7* and *fat-5* (another SBP-1 responsive gene) in the reporter strain and also analyzed *fat-7* and *fat-5* expression in wild-type animals. First, we confirmed that five of the top ten class 1 genes were necessary for *pfat-7::GFP* mRNA expression (see Table S1; see columns K–M for validation). For class 2 genes, we found that only *lpin-1*, *arf-1.2*, and *plc-1* RNAi increased *gfp*, endogenous *fat-7* and *fat-5* mRNA levels (Figures S1B and S1D). *lpin-1*, *arf-1.2*, and *plc-1* RNAi also decreased *gfp* levels in the low-PC *sams-1(lf);pfat-7::GFP* (Figures S1C and S1E). Finally, while *lpin-1* and *arf-1.2* RNAi increased endogenous *fat-7* and *fat-5* in wild-type worms, *plc-1* effects occurred only in the transgenic strain (Figure S1D). We also noted that *sams-1(lf)* animals with reduced *lpin-1* showed additional phenotypes, including slowed development and synthetic lethality (Figure S1G).

The importance of *lpin-1* for low-PC activation *pfat-7::GFP* prompted us to examine pathways producing the LPIN-1 substrate, PA. *C. elegans* contains multiple paralogs of PA synthesis genes (Figure S1A): three GPATs, *acl-4*, -5 and -6 and two AGPATs, *acl-11* and *acl-13* (Ohba et al., 2013). Our screen data showed that one GPAT (*acl-4*) and one AGPAT (*acl-11*) were required for *pfat-7::GFP* expression in wild-type, but not in *sams-1(lf)* animals (Figure 1C). In validation assays, we found GFP was lower after *acl-4* or *acl-11* RNAi (Figure S2A), as were *gfp* and endogenous *fat-7* mRNA levels (Figure S2B). *pfat7::gfp* or endogenous *fat-7* gene expression was not altered by *acl-4* and *acl-11* RNAi in low-PC (*sams-1(lf);pfat-7::GFP*) conditions (Figures S2C and S2D).

***sams-1* or *lpin-1* RNAi Reduce DAG and Change PA/PC Ratios in *C. elegans* Microsomal Membranes**

Loss of *sams-1* decreases PC and increases TAG (Ding et al., 2015; Walker et al., 2011); however, *lpin-1* knockdown is predicted to affect PA and DAG (Figure S1A). To generate lipid profiles in membranes linked to SBP-1/SREBP-1 processing, we profiled microsomal lipids from *sams-1* or *lpin-1* RNAi animals. We validated fractionations by immunoblotting with *C. elegans* ER or Golgi specific antibodies (Figure S3A). LC/MS analysis identified over 1,600 lipid species in over 20 classes (Table S2). Principal component analysis shows that control, *sams-1*, and *lpin-1* RNAi samples are distinct and that biological

replicates are similar (Figure S3B). We analyzed the data in two ways: first, values for lipid species were totaled for each class and second, the distribution of species within each class was determined. In *sams-1(RNAi)* microsomal fractions, we found that TAGs as a class were increased and PCs as a class were decreased (Figures S2C and S2D; see Table S2 for statistics), as in our previous studies analyzing whole-worm extracts by GC/MS (Ding et al., 2015; Walker et al., 2011). Many other lipid species also changed (Figure S3E; Table S2), perhaps in response to synthetic links between PC and other lipids. We were surprised to see that DAG as a class was similar to wild-type; however, many individual species shifted significantly lower and the distribution of species within the class differed significantly after *sams-1(RNAi)* (Figure S3F; Table S2). This is in contrast to models for PC metabolism that predict increased DAG when PC synthesis is blocked (Sarri et al., 2011) and may reflect the specific nature of our assay.

lpin-1 RNAi, on the other hand, had fewer overall effects, primarily lowering levels of many DAG species and increasing multiple PA species (Figures S3F–S3I; see Table S2 for statistics), consistent with a role for *lpin-1* as a PA phosphatase. Finally, we noted two major similarities in *sams-1* and *lpin-1* lipid profiles. First, ratios of PA/PC species were elevated, and, second, the distribution of species within the DAG class shifted significantly lower. This is consistent with our genetic evidence implicating enzymes directly linked to PA, DAG, and PC in the regulation of *pfat-7::GFP*.

***lpin-1* and *arf-1.2* Are Important for low-PC Effects on SBP-1**

Increased *fat-7* expression after *lpin-1* RNAi suggests SBP-1 may be more active. To determine whether maturation was stimulated, we examined subcellular localization of intestinal GFP::SBP-1 (Walker et al., 2010). Similar to *sams-1* RNAi, knockdown of either *lpin-1* or *arf-1.2* resulted in increased nuclear levels of GFP::SBP-1 (Figure 2A), along with increases in *fat-7* and *fat-5* (Figure 2B). Interestingly, we noted that *lpin-1* expression was slightly increased after *sams-1* RNAi (Figure 2B; see also Ding et al., 2015). Finally, depletion of PA synthesis enzymes *acl-4* and *acl-11* had opposite effects, decreasing nuclear SBP-1 (Figures S2E–S2G).

Next, we performed Sudan Black staining to gauge size and distribution of lipid droplets and measured TAG for total levels. To avoid confounding results from the developmental delay of *sams-1(lf); lpin-1(RNAi)* animals (Figure S1G), PC production was rescued with choline until the L3 stage (Ding et al., 2015); growth without choline after L3 was sufficient to increase SBP-1-dependent gene expression (Figure S1H). *lpin-1* RNAi animals appeared clear with slightly reduced Sudan Black staining (Figures 2C and 2D), consistent with reports of decreased Nile Red (Golden et al., 2009; Zhang et al., 2013); however, TAG stores were not reduced in colorimetric assays (Figure 2E) or microsomal extracts (Table S2, see tab:TG.class). This suggests other mechanisms may compensate for LPIN-1 function in TAG synthesis. Importantly, large lipid droplets in *sams-1(lf)* animals decreased upon *lpin-1* RNAi and TAG returned close to wild-type levels (Figures 2C–2E). Thus, interference with both *sams-1* and *lpin-1* rescues effects of low-PC on stored lipids.

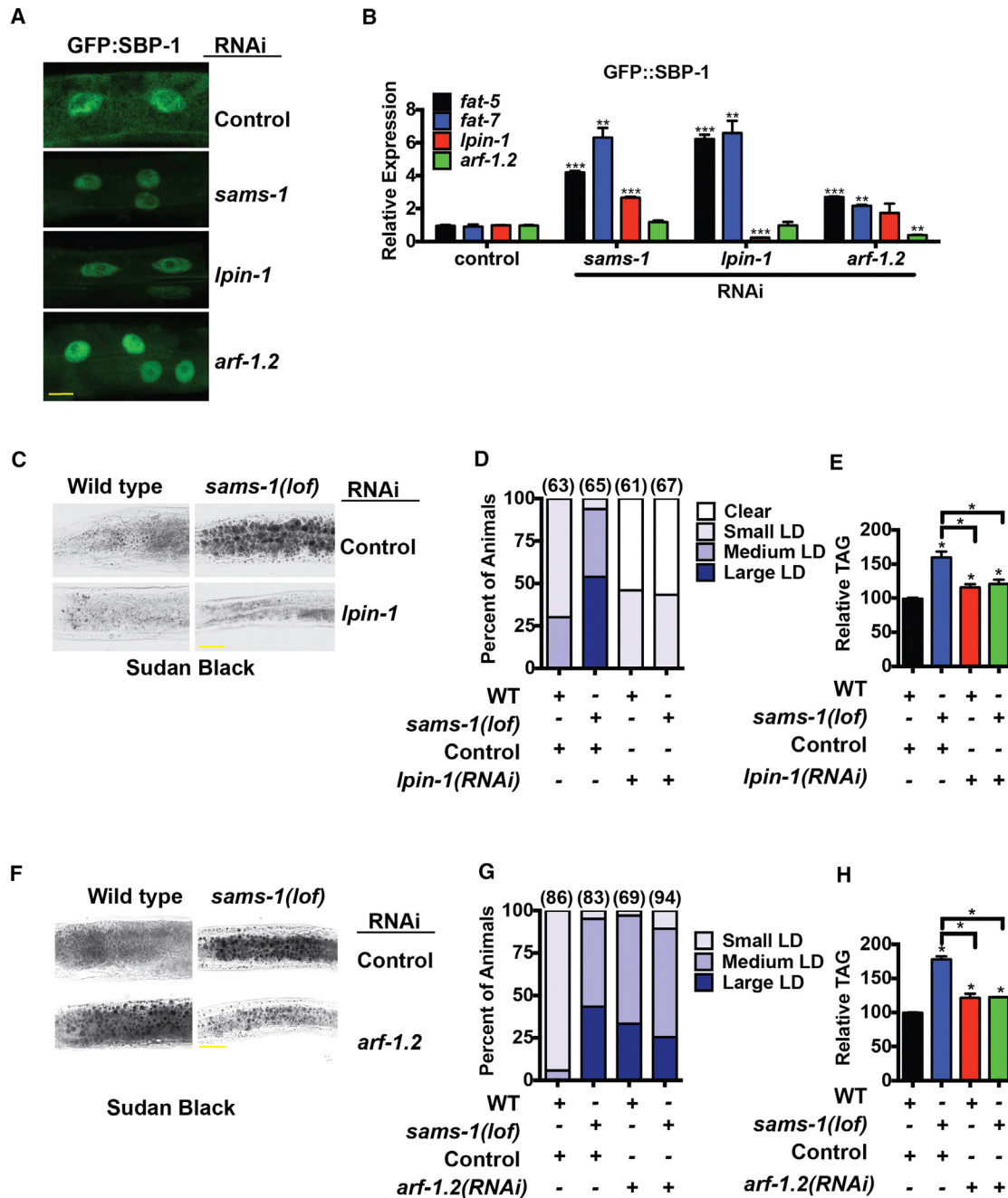


Figure 2. In *C. elegans*, *lpin-1* and *arf-1.2* RNAi Increase Nuclear Localization of SBP-1::GFP and Are Important for Lipid Accumulation in *sams-1(lol)* Animals

(A) Confocal projection showing nuclear accumulation of intestinal GFP::SBP-1 after *sams-1*, *lpin-1*, or *arf-1.2* RNAi. Scale bar, 10 μ m.

(B) qRT-PCR showing upregulation of *fat-5* and *fat-7*.

(C-E) Lipid accumulation when *sams-1* and *lpin-1* where co-depleted assessed by Sudan Black staining (C) with quantitation of percent of animals stained (D) or TAG level (E). Scale bar for Sudan Black, 25 μ m.

(F–H) For *sams-1* and *arf-1.2* co-depletion, Sudan Black staining and quantitation are in (F) and (G), and TAG measurements are in (H). Number of animals is shown in parentheses.

Error bars show SD. Results from Student's t test shown by * $p < 0.05$, ** $p < 0.01$, *** $p < 0.005$. See also Table S2 and Figure S2.

arf-1.2 knockdown also increased *fat-7* expression and nuclear localization of GFP::SBP-1 (Figures 2A and 2B). Therefore, we assessed Sudan Black staining and TAG levels. *arf-1.2(RNAi)* worms had an increase in lipid droplets (Figures 2F and 2G); however, TAG levels were only slightly higher than wild-type (Figure 2H), suggesting effects on droplets size and not total lipid levels. This is consistent with reports of ARF function in lipid droplet formation (Wilfling et al., 2014). In contrast, *arf-1.2 RNAi* reduced lipid droplet appearance, number, and overall TAG levels in *sams-1(lf)* animals. Taken together, our *C. elegans* studies show that reducing function of LPIN-1, an enzyme converting PA to DAG, limits low-PC activation of SBP-1/SREBP. Thus, enzymes that produce or utilize PA may be a key to this mechanism.

***LPIN1* Knockdown Is Sufficient to Activate Mammalian SREBP-1 and Necessary for Low-PC Effect**

In mammals, interference with PC synthesis results in hepatosteatosis (Vance, 2014), as SREBP-1-dependent lipogenesis programs are stimulated (Walker et al., 2011). To determine whether Lipin 1 was required for activation of mammalian SREBP-1 in this context, we depleted *LPIN1* with small interfering RNA (siRNA). Like knockdown of *PCTY1a/CCTa*, the rate limiting enzyme in mammalian PC production, *LPIN1* depletion increased levels of mature, nuclear SREBP-1 (Figures 3A–3C). *LPIN1* knockdown also increased nuclear localization and proteolytic maturation of a N-terminal HA tagged SREBP-1 (Figure 3D; Figures S4A and S4B). siRNA-mediated depletion was confirmed by qRT-PCR and immunoblots from Dignam extracts of HepG2 cells (Figures S4C and S4D).

To determine whether *LPIN1* function was important for low-PC effects on SREBP-1, we used siRNA to deplete both *PCTY1a* and *LPIN1* in HA-SREBP-1 lines. For combined siRNA, we kept RNA amounts constant with scrambled control and achieved efficient knockdown for both *PCTY1a* and *LPIN1* (Figure S4C). We found that nuclear HA-SREBP-1 localization was lost in *PCTY1a* / *LPIN1* double knockdowns (Figures 3D and 3F), suggesting that, as in *C. elegans*, *LPIN1* knockdown abrogates the low-PC effect on SREBP-1. Similar effects were seen with endogenous SREBP-1 (Figures S4E and S4F).

Lipin 1 converts PA to DAG, thus lower activity predicts increases in PA (Takeuchi and Reue, 2009). To determine whether exogenous PA could recapitulate *LPIN1* effects, we treated HA-SREBP-1 cells with PA and found that indeed, SREBP-1 nuclear accumulation increased (Figures 3E and 3G). Further paralleling *LPIN1* knockdown, PA decreased nuclear SREBP-1 in *PCTY1a* siRNA cells (Figures 3E and 3G). Although effects of exogenous PA on cultured cells may be complex and have species dependent effects, changes in SREBP-1 maturation are consistent with effects of *LPIN1* knockdown. We also investigated low-PC induced lipid droplet formation and found that, as in *C. elegans*, co-depletion of *PCTY1a* with *LPIN1* restored lipid droplets to wild-type levels (Figures S4G–S4I). Taken together, our results suggest that inhibiting *LPIN1* expression or adding its exogenous substrate can reverse the effects of *PCYT1a* knockdown on SREBP-1.

Lipin 1 has been shown to inhibit SREBP-1 activity when mTORC1-dependent (mechanistic Target of Rapamycin Com-

plex) phosphorylation decreases and it localizes to the nucleus, sequestering SREBP-1 at the nuclear membrane. However, mechanisms linking low-PC SREBP-1 activation to Lipin 1 appear distinct. First, SREBP-1 nuclear localization after *PCTY1a* or *LPIN1* knockdown is nucleoplasmic and target genes are activated (see also Walker et al., 2011). Second, localization of endogenous Lipin 1 (Figures S5A and S5B; specificity antibody shown in Figure S5C), or a transfected Flag-Lipin 1 (Figure S5D) is not changed after *PCTY1a* knockdown. Finally, fractionation experiments show similar levels of Lipin 1 isoforms in nuclear/ER and microsomal fractions in control and *PCTY1a* extracts (Figure S5E). Lipin 1 may also act in co-activation of β-oxidation genes (Reue and Zhang, 2008); however, these genes are not altered upon *PCYT1a* depletion (Figure S5F). Thus, mechanisms linking Lipin 1 and SREBP-1 in low PC appear distinct from mTORC1-mediated control of Lipin 1 localization or direct effects on gene regulation.

***PCTY1a* and *LPIN1* Knockdown Affect ARF1 Activity**

Our previous studies found that low-PC or disruptions in ARF1 GEF (Guanine Exchange Factor) GEF1 induced maturation of SREBP-1 (Walker et al., 2011), and our *C. elegans* screen also implicated *arf-1.2* in SBP-1 activation (Figures 1D, 1F, and 2A). To determine whether this mechanism extended to mammalian cells, we examined SREBP-1 localization and processing in HepG2 cells after ARF1 siRNA and found that nuclear accumulation increased and processed SREBP-1 appeared at higher levels (Figures 3H–3J).

The validated hits from our *C. elegans* screen strongly implicated enzymes that alter PA or DAG levels in low-PC mediated processing of SREBP-1. Interestingly, both PA and DAG have been reported to affect ARF1 function, interfering with COP I transport (Asp et al., 2009; Fernández-Ulibarri et al., 2007; Manifava et al., 2001). Therefore, we asked whether knockdown of *LPIN1* or *PCYT1a* affected levels of active, GTP-bound ARF1 and found that, strikingly, levels were diminished in both instances (Figures 4A–4C). As in our previous assays, double knockdown of *LPIN1* and *PCYT1a* corrected defects (Figures 4D and 4E). Finally, we asked whether exogenous PA would phenocopy *LPIN1* knockdown and rescue *siPCYT1a* effects on GTP-ARF1 levels and found partial rescue of active ARF1 (Figures 4F and 4G).

Cytosolic membrane levels of PA (Csaki et al., 2013), DAG (Sarri et al., 2011), or PC (Vance, 2014) could be affected in either *LPIN1* or *PCYT1a* knockdown. Interestingly, ARF1 activity depends on membrane recruitment of the GTPase itself along with membrane association of the GAP (GTPase Activating Protein, ARFGAP1) and GEF (GEF1) (Bankaitis et al., 2012; Lev, 2006; Spang, 2002). In addition, DAG levels may be important for ARFGAP1 association (Antony et al., 1997; Bigay et al., 2003; Fernández-Ulibarri et al., 2007). Therefore, we compared association of ARF1, GEF1, or ARFGAP1 with microsomal membranes after *PCYT1a* or *LPIN1* siRNA. Strikingly, GEF1 association was broadly decreased, while ARFGAP1 and ARF1 did not change (Figures 4H and 4I; Figures S5G and S5H). This suggests that local changes in membrane lipids that occur after *PCYT1a* or *LPIN1* depletion may have profound effects on recruitment GEF1, leading to disruptions in ARF1 activity activating SREBP-1.

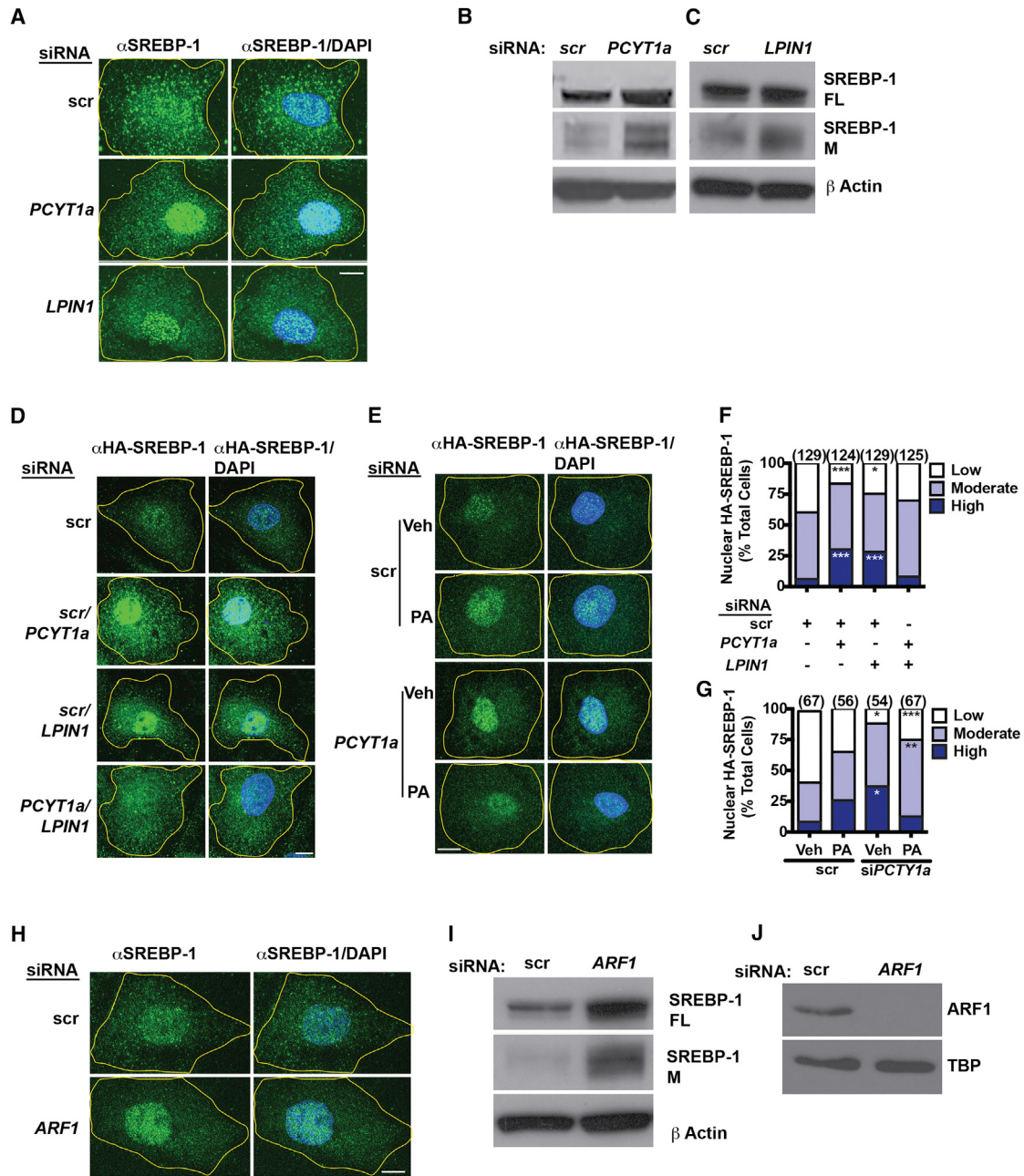


Figure 3. siRNA Knockdown of LPIN1 Is Similar to PCYT1 Depletion, Increasing SREBP-1 Nuclear Accumulation in Human Cells

(A–C) Confocal projections of immunostaining of endogenous SREBP-1 (A) or immunoblots (B and C) showing accumulation of the nuclear, processed form after siRNA of PCYT1a or LPIN1 in HepG2 cells. scr is the scrambled siRNA control, and yellow lines show cell boundaries. FL shows the full-length SREBP-1 precursor, and M is the mature, cleaved version.

(D and F) Confocal projections of HA-SREBP-1 levels after double knockdown of PCYT1 and LPIN1 in HepG2 cells (D) with quantitation in (F).

(E and G) Immunostaining and confocal projection of HepG2 cells shows increased nuclear accumulation of HA-SREBP-1 in cells treated with phosphatidic acid (PA). PA treatment decreases nuclear HA-SREBP-1 in siPCYT1a knockdown cells. Quantitation is in (G).

(H and I) Endogenous SREBP-1 localization is shown by confocal projections of immunostaining (H) or by immunoblot (I) after treatment of HepG2 cells with siRNA to ARF1. scr is scrambled control and yellow lines show cell outlines.

(J) Immunoblots show decrease in ARF1 after siRNA treatment. Number of cells are shown in parenthesis.

Results from Student's t test shown by *p < 0.05, **p < 0.01, ***p < 0.005. Scale bars, 10 μ m. See also Table S3 and Figures S4 and S5.

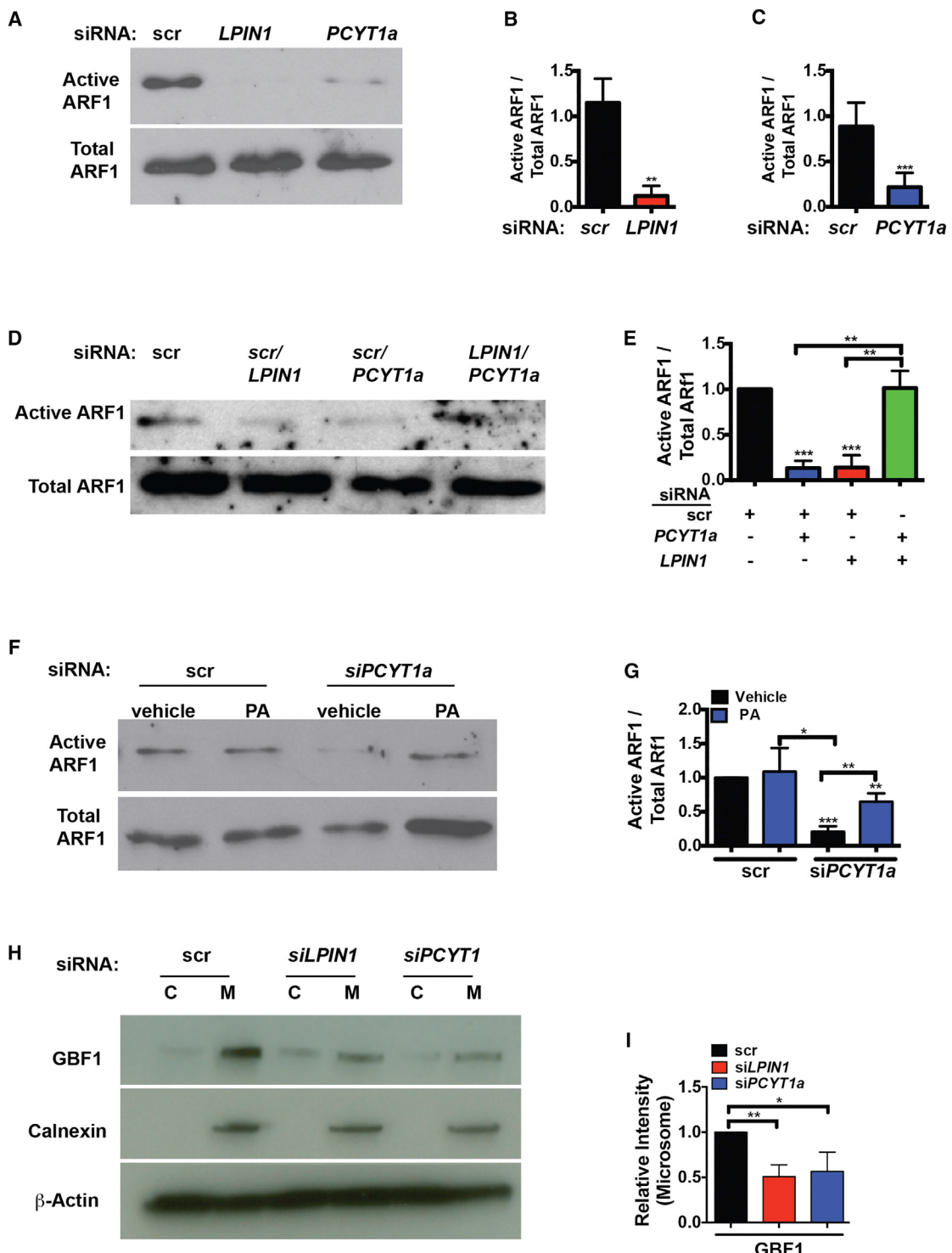


Figure 4. Knockdown of Mammalian *PCTY1* or *LPIN1* Decreases ARF1 Activity

(A) Pull-down assays specific for GTP-bound ARF1 show significant decreases after *LPIN1* or *PCTY1a* knockdown.
(B and C) Densitometry showing an average of three experiments for *siLPIN1* or five experiments for *siPCTY1a* is shown in (B) and (C), respectively.
(D and E) Comparison of active ARF1 levels shown in a representative immunoblot (D) or by densitometry from immunoblots of the double knockdown of *PCTY1a* and *LPIN1* (E).
(F and G) Assessment of active ARF1 levels after *PCTY1a* siRNA or treatment with PA shown by immunoblot (F) or by densitometry (G).

(legend continued on next page)

DISCUSSION

Lipid storage requires coordinated production of fatty acids, phospholipids, TAGs, and other complex lipids (Horton et al., 2002). Many of these lipids also function in membrane structure or as signaling effectors, thus regulators of lipogenesis may respond to various signals. Our screen identified *lpin-1*, a PA phosphatase, (Takeuchi and Reue, 2009) as an activator of SBP-1/SREBP-1. Although enzymatic activities of lipins suggest straightforward synthetic functions, they have diverse roles and broad physiological effects (Csaki et al., 2013). For example, the *fld* mouse model of *LPIN1* deficiency has metabolic defects including fatty liver and lipodystrophy (Péterfy et al., 2001) and the SREBP-1 transcriptional target SCD1 is up-regulated (Chen et al., 2008). Lipin 1 has also been reported to affect SREBP-1 activity through nuclear membrane sequestration (Peterson et al., 2011) or to act as a co-activator of β-oxidation genes with PPARα (Finck et al., 2006); however, neither of these activities was altered after *PCYT1/CCTa* knockdown. In this context, we hypothesize Lipin 1-dependent effects on SREBP-1 occur when changes in membrane lipids alter membrane:protein interactions and activity of GBF-1 and ARF-1.

Changes in PA, DAG, or PC within subcellular membranes could have multiple effects. However, our data suggested a connection to ARFs. Notably, several studies have found that DAGs are important for ARF1 function or for recruiting ARFGAP (Antonny et al., 1997; Bigay et al., 2003; Fernández-Ulibarri et al., 2007; Randazzo and Kahn, 1994). However, we found that it was the ARF-GEF, GBF1, that bound less well to membranes after *PCYT1* or *LPIN1* knockdown. Loss of GBF1 activates the unfolded protein response and promotes cell death in mammalian cells (Citterio et al., 2008) and defects in development and Golgi integrity in *C. elegans* (Ackema et al., 2013). However, larval growth arrest after *gbf-1(RNAi)* in our screen precluded analysis. A recent study has suggested that GBF1 is recruited to membranes in response to increases in ARF-GDP (Quilty et al., 2014). We hypothesize that local changes in ratios of PA to PC species or decreases in DAG species, as seen in our studies of *C. elegans* microsomes, limit GBF1 recruitment and prevent generation of GTP-bound ARF1. In this instance, there could be insufficient DAG for recruitment or changes in curvature predicted by a PA-rich membrane could disrupt membrane:protein interactions.

Finally, we have found that co-depletion of PC biosynthetic enzymes and *lpin-1/LPIN1* returns SBP-1/SREBP-1 function to basal levels and restores TAG levels. In this case, inhibiting the PA to DAG transition could limit both TAG and PC. We hypothesize this allows levels to rebalance, restoring ARF1 function and baseline SBP-1/SREBP-1 activity. Thus, our results suggest SBP-1/SREBP-1 transcriptional programs favoring lipogenesis may be stimulated when the balance of PA, DAG, or PC change within microsomal membranes.

EXPERIMENTAL PROCEDURES

***C. elegans*: Strains and RNAi Constructs**

Nematodes were cultured using standard *C. elegans* methods. For information on strains and RNAi constructs, see Table S3.

***C. elegans*: RNAi Screen**

L1 larva were plated into 96-well plates arrayed with RNAi bacteria and scored at the L4/young adult transition. Each well was given a score from -3 to +3 with 0 as no change in four independent replicates and scores were averaged. RNAi clones whose average scores were >0.7 or <-0.7 were selected as candidates for validation.

***C. elegans*: GFP Visualization**

pfat-7::GFP and *SBP-1::GFP* *C. elegans* strains were grown until the L4/young adult transition, and images were acquired on a Leica SPE II confocal microscope. All images were taken at identical gain settings within experimental sets, and Adobe Photoshop was used for corrections to levels across experimental sets.

***C. elegans*: Gene Expression Analysis**

C. elegans at the L4/young adult transition were lysed and qRT-PCR analysis was performed as in Ding et al. (2015). Primers are available upon request.

***C. elegans*: Lipid Analysis**

C. elegans were grown on plates containing 30 mM choline until L2, washed, and transferred to plates without choline until the second day of adulthood. Sudan Black staining was performed as in Ding et al. (2015). Briefly, animals were dehydrated in ethanol, stained with Sudan Black, placed on agar pads, and photographed in bright-field microscopy with a Leica SPE II. Sudan Black staining was quantitated by blind scoring of more than 30 for of small, medium, or large lipid droplets. TAG levels were determined using a Triglyceride Colorimetric Assay Kit (Cayman Chemical, 10010303) following manufacturer's instructions. For quantitation of TAG levels, two-tailed Student's t tests were used to determine significance between three biological replicates. For lipidomic methods, see Supplemental Experimental Procedures.

Cell Culture: Media and Stable Cell Lines

HepG2 cells (ATCC, HB-8065) were maintained in Minimum Essential Medium (Invitrogen) supplemented with 10% FBS (Invitrogen), glutamine (Invitrogen), and sodium pyruvate (Invitrogen). HepG2 cells stably expressing human SREBP-1c were generated by transfection of a pCMV6 SREBP-1c with an N-terminal hemagglutinin (HA) epitope tag (Origene, RC208404) and selection with Geneticin (Invitrogen).

Cell Culture: Transfection and siRNA

siRNA oligonucleotides were transfected for 48 hr with Lipofectamine RNAiMAX Transfection Reagent (Invitrogen, 13778100) (see Table S3 for specific siRNAs). Cells were incubated for 16 hr in 1% Lipoprotein Deficient Serum (LDS) (Biomedical Technologies, BT907) and 25 µg/ml ALLN (Calbiochem) for 30 min prior to harvesting. For studies with co-depletion of *PCYT1a* and *LPIN1*, equal amounts of each siRNA or targeting plus scrambled were transfected.

Cell Culture: Gene Expression

Total mRNA was extracted from with Tri-Reagent according to manufacturer's protocol (Sigma). qRT-PCR conditions were identical to *C. elegans* studies. For qRT-PCR studies, graphs represent representative experiments selected from at least three biological replicates. Two-tailed Student's t tests were used to compare significance between values with two technical replicates. Primer sequences are available upon request.

(H and I) Immunoblots of fractionated HepG2 cells comparing cytosolic (C) to microsomal (M) association of GBF1 or ARF1 after knockdown of *PCYT1a* or *LPIN1*. Calnexin shows membrane-associated fractions and β-actin confirms loading. For densitometry (I), values were normalized to vehicle-treated scrambled (scr) expressing cells and represent three independent experiments.

Error bars show SD. Results from Student's t test shown by *p < 0.05, **p < 0.01, ***p < 0.005 compared to scrambled (scr) conditions. ns, not significant.

Lipid Vesicle Formation

Lipid vesicles containing 1,2-dipalmitoyl-sn-glycero-3-phosphate (PA) (Avanti Polar Lipids, 830855P) were prepared by water bath sonication as in [Zhang et al. \(2012\)](#) and added at final concentrations of 100 μM during the 16 hr incubation in 1% LDS.

Immunofluorescence and Oil Red O Staining

Transfected cells were fixed in 3.7% paraformaldehyde and permeabilized in 0.5% NP-40 prior to blocking in 5% fetal bovine serum/ 0.1% NP-40 and antibody treatment. For oil red O, cells were fixed with 3.7% paraformaldehyde, stained with oil red O (3 mg/ml in 60% isopropanol) for 10 min, and visualized. For quantification of antibody staining or lipid droplets, ten individual focal areas were photographed and then scored blind for high, medium, or low nuclear accumulation (antibody) or analyzed using BioPix iQ 2.1.4 (droplets). Two-tailed Student's t tests were used to compare significance between the ten photographed areas and are representative of three biological replicates. All images within experimental sets were taken with a Leica SPE II at identical confocal gain settings and Adobe Photoshop was used for levels corrections.

Immunoblot Analysis

Cells were lysed by syringe in high-salt RIPA (50 mM Tris [pH 7.4]; 400 mM NaCl; 0.1% SDS; 0.5% NaDeoxycholate; 1% NP-40; 1 mM DTT, 2.5 μg/ml ALLN, Complete protease inhibitors [Roche]). Extracts were separated on Invitrogen NuPage gels (4%-12%), transferred to nitrocellulose, and probed with specified antibodies. Immune complexes were visualized with Luminol Reagent (Millipore). Densitometry was performed by scanning of the film, and then analysis of pixel intensity was performed with ImageJ software. Graphs show average of at least three independent experiments with control values normalized to one.

Cell Fractionation: HepG2

Transfected cells were resuspended in cold homogenization buffer (Microsome purification kit, Biovision) and dounced and then cleared briefly. Supernatants were centrifuged at 80,000 × g for 45 min. Pellets were collected as microsomal fractions with the supernatant designated as the cytosolic fraction.

Active Arf1 Analysis

Levels of active Arf1 were analyzed using an Active Arf1 Pull-Down and Detection Kit (Thermo Scientific) following manufacturer's instructions. Densitometry was performed by scanning of the film, and then analysis of pixel intensity with ImageJ software was performed. Graphs show average of at least three independent experiments with control values normalized to one.

SUPPLEMENTAL INFORMATION

Supplemental Information includes Supplemental Experimental Procedures, five figures, and three tables and can be found with this article online at <http://dx.doi.org/10.1016/j.celrep.2016.05.086>.

AUTHOR CONTRIBUTIONS

Conceptualization and Methodology, A.K.W.; Software, S.G. and Y.J.K.E.; Validation, L.J.S., W.D., and A.K.W.; Formal Analysis, L.J.S. and A.K.W.; Investigation, L.J.S., W.D., and A.K.W.; Writing—Original Draft, Writing—Reviewing and Editing, and Visualization, Supervision, Project Administration, and Funding Acquisition, A.K.W.

ACKNOWLEDGMENTS

We thank Drs. David Lambright (UMASS Medical School) and Stefan Taubert (University of British Columbia) for reading of the manuscript as well as Drs. Marian Walhout (UMASS Medical School), Victor Ambros (UMASS Medical School), Michael Czech (UMASS Medical School), Michelle Mondoux (College of the Holy Cross), and members of their labs for helpful discussion. We also

thank Dr. Michael Lee (UMASS) for advice on bioinformatics. Some *C. elegans* strains were provided by the *Caenorhabditis* Genetics Center (CGC), which is funded by NIH Office of Research Infrastructure Programs (P40 OD010440). This work was supported by the NIH through R01DK084352 to A.K.W.

Received: September 21, 2015

Revised: April 29, 2016

Accepted: May 22, 2016

Published: June 16, 2016

REFERENCES

- Ackema, K.B., Sauder, U., Solinger, J.A., and Spang, A. (2013). The ArfGEF GBF-1 is required for ER structure, secretion and endocytic transport in *C. elegans*. *PLoS ONE* 8, e67076.
- Antony, B., Huber, I., Paris, S., Chabre, M., and Cassel, D. (1997). Activation of ADP-ribosylation factor 1 GTPase-activating protein by phosphatidylcholine-derived diacylglycerols. *J. Biol. Chem.* 272, 30848–30851.
- Asp, L., Kartberg, F., Fernandez-Rodriguez, J., Smedh, M., Elsner, M., Laporte, F., Bárcena, M., Jansen, K.A., Valentijn, J.A., Koster, A.J., et al. (2009). Early stages of Golgi vesicle and tubule formation require diacylglycerol. *Mol. Biol. Cell* 20, 780–790.
- Bankaitis, V.A., Garcia-Mata, R., and Mousley, C.J. (2012). Golgi membrane dynamics and lipid metabolism. *Curr. Biol.* 22, R414–R424.
- Bigay, J., Gounon, P., Robineau, S., and Antonny, B. (2003). Lipid packing sensed by ArfGAP1 couples COPI coat disassembly to membrane bilayer curvature. *Nature* 426, 563–566.
- Brown, M.S., and Goldstein, J.L. (1997). The SREBP pathway: regulation of cholesterol metabolism by proteolysis of a membrane-bound transcription factor. *Cell* 89, 331–340.
- Chen, Z., Gropler, M.C., Norris, J., Lawrence, J.C., Jr., Harris, T.E., and Finck, B.N. (2008). Alterations in hepatic metabolism in fld mice reveal a role for lipin 1 in regulating VLDL-triacylglyceride secretion. *Arterioscler. Thromb. Vasc. Biol.* 28, 1738–1744.
- Citterio, C., Vichi, A., Pacheco-Rodriguez, G., Aponte, A.M., Moss, J., and Vaughan, M. (2008). Unfolded protein response and cell death after depletion of brefeldin A-inhibited guanine nucleotide-exchange protein GBF1. *Proc. Natl. Acad. Sci. USA* 105, 2877–2882.
- Csaki, L.S., Dwyer, J.R., Li, X., Nguyen, M.H., Dewald, J., Brindley, D.N., Lusis, A.J., Yoshinaga, Y., de Jong, P., Fong, L., et al. (2013). Lipin-1 and lipin-3 together determine adiposity in vivo. *Mol. Metab.* 3, 145–154.
- DeBose-Boyd, R.A., Brown, M.S., Li, W.P., Nohturfft, A., Goldstein, J.L., and Espenshade, P.J. (1999). Transport-dependent proteolysis of SREBP: relocation of site-1 protease from Golgi to ER obviates the need for SREBP transport to Golgi. *Cell* 99, 703–712.
- Ding, W., Smulan, L.J., Hou, N.S., Taubert, S., Watts, J.L., and Walker, A.K. (2015). s-adenosylmethionine levels govern innate immunity through distinct methylation-dependent pathways. *Cell Metab.* 22, 633–645.
- Fernández-Ulibarri, I., Vilella, M., Lázaro-Diézquez, F., Sarri, E., Martínez, S.E., Jiménez, N., Claro, E., Mérida, I., Burger, K.N., and Egea, G. (2007). Diacylglycerol is required for the formation of COPI vesicles in the Golgi-to-ER transport pathway. *Mol. Biol. Cell* 18, 3250–3263.
- Finck, B.N., Gropler, M.C., Chen, Z., Leone, T.C., Croce, M.A., Harris, T.E., Lawrence, J.C., Jr., and Kelly, D.P. (2006). Lipin 1 is an inducible amplifier of the hepatic PGC-1alpha/PPARalpha regulatory pathway. *Cell Metab.* 4, 199–210.
- Golden, A., Liu, J., and Cohen-Fix, O. (2009). Inactivation of the *C. elegans* lipin homolog leads to ER disorganization and to defects in the breakdown and reassembly of the nuclear envelope. *J. Cell Sci.* 122, 1970–1978.
- Goldstein, J.L., DeBose-Boyd, R.A., and Brown, M.S. (2006). Protein sensors for membrane sterols. *Cell* 124, 35–46.
- Horton, J.D. (2002). Sterol regulatory element-binding proteins: transcriptional activators of lipid synthesis. *Biochem. Soc. Trans.* 30, 1091–1095.

- Horton, J.D., Goldstein, J.L., and Brown, M.S. (2002). SREBPs: activators of the complete program of cholesterol and fatty acid synthesis in the liver. *J. Clin. Invest.* **109**, 1125–1131.
- Kamath, R.S., Fraser, A.G., Dong, Y., Poulin, G., Durbin, R., Gotta, M., Kapanin, A., Le Bot, N., Moreno, S., Sohrmann, M., et al. (2003). Systematic functional analysis of the *Caenorhabditis elegans* genome using RNAi. *Nature* **421**, 231–237.
- Lev, S. (2006). Lipid homeostasis and Golgi secretory function. *Biochem. Soc. Trans.* **34**, 363–366.
- Manifava, M., Thuring, J.W., Lim, Z.Y., Packman, L., Holmes, A.B., and Ktistakis, N.T. (2001). Differential binding of traffic-related proteins to phosphatidic acid- or phosphatidylinositol (4,5)-bisphosphate-coupled affinity reagents. *J. Biol. Chem.* **276**, 8987–8994.
- Ohba, Y., Sakuragi, T., Kage-Nakadai, E., Tomioka, N.H., Kono, N., Imae, R., Inoue, A., Aoki, J., Ishihara, N., Inoue, T., et al. (2013). Mitochondria-type GPAT is required for mitochondrial fusion. *EMBO J.* **32**, 1265–1279.
- Osborne, T.F., and Espenshade, P.J. (2009). Evolutionary conservation and adaptation in the mechanism that regulates SREBP action: what a long, strange tRIP it's been. *Genes Dev.* **23**, 2578–2591.
- Péterfy, M., Phan, J., Xu, P., and Reue, K. (2001). Lipodystrophy in the fld mouse results from mutation of a new gene encoding a nuclear protein, lipin. *Nat. Genet.* **27**, 121–124.
- Peterson, T.R., Sengupta, S.S., Harris, T.E., Carmack, A.E., Kang, S.A., Balderas, E., Guertin, D.A., Madden, K.L., Carpenter, A.E., Finck, B.N., and Sabatini, D.M. (2011). mTOR complex 1 regulates lipin 1 localization to control the SREBP pathway. *Cell* **146**, 408–420.
- Quilty, D., Gray, F., Summerfeldt, N., Cassel, D., and Melançon, P. (2014). Arf activation at the Golgi is modulated by feed-forward stimulation of the exchange factor GBF1. *J. Cell Sci.* **127**, 354–364.
- Randazzo, P.A., and Kahn, R.A. (1994). GTP hydrolysis by ADP-ribosylation factor is dependent on both an ADP-ribosylation factor GTPase-activating protein and acid phospholipids. *J. Biol. Chem.* **269**, 10758–10763.
- Reue, K. (2007). The role of lipin 1 in adipogenesis and lipid metabolism. *Novartis Found. Symp.* **286**, 58–68; discussion 68–71, 162–163, 196–203.
- Reue, K., and Zhang, P. (2008). The lipin protein family: dual roles in lipid biosynthesis and gene expression. *FEBS Lett.* **582**, 90–96.
- Rual, J.F., Ceron, J., Koreth, J., Hao, T., Nicot, A.S., Hirozane-Kishikawa, T., Vandenhoute, J., Orkin, S.H., Hill, D.E., van den Heuvel, S., and Vidal, M. (2004). Toward improving *Caenorhabditis elegans* phenome mapping with an ORFeome-based RNAi library. *Genome Res.* **14** (10B), 2162–2168.
- Sarri, E., Sicart, A., Lázaro-Díéguez, F., and Egea, G. (2011). Phospholipid synthesis participates in the regulation of diacylglycerol required for membrane trafficking at the Golgi complex. *J. Biol. Chem.* **286**, 28632–28643.
- Spang, A. (2002). ARF1 regulatory factors and COPI vesicle formation. *Curr. Opin. Cell Biol.* **14**, 423–427.
- Takeuchi, K., and Reue, K. (2009). Biochemistry, physiology, and genetics of GPAT, AGPAT, and lipid enzymes in triglyceride synthesis. *Am. J. Physiol. Endocrinol. Metab.* **296**, E1195–E1209.
- Vance, D.E. (2014). Phospholipid methylation in mammals: from biochemistry to physiological function. *Biochim. Biophys. Acta* **1838**, 1477–1487.
- Walker, A.K., Yang, F., Jiang, K., Ji, J.-Y., Watts, J.L., Purushotham, A., Boss, O., Hirsch, M.L., Ribich, S., Smith, J.J., et al. (2010). Conserved role of SIRT1 orthologs in fasting-dependent inhibition of the lipid/cholesterol regulator SREBP. *Genes Dev.* **24**, 1403–1417.
- Walker, A.K., Jacobs, R.L., Watts, J.L., Rottiers, V., Jiang, K., Finnegan, D.M., Shioda, T., Hansen, M., Yang, F., Niebergall, L.J., et al. (2011). A conserved SREBP-1/phosphatidylcholine feedback circuit regulates lipogenesis in metazoans. *Cell* **147**, 840–852.
- Wilfling, F., Thiam, A.R., Olarte, M.J., Wang, J., Beck, R., Gould, T.J., Allgeyer, E.S., Pincet, F., Bewersdorf, J., Farese, R.V., Jr., and Walther, T.C. (2014). Arf1/COPI machinery acts directly on lipid droplets and enables their connection to the ER for protein targeting. *eLife* **3**, e01607.
- Yang, F., Vought, B.W., Satterlee, J.S., Walker, A.K., Jim Sun, Z.-Y., Watts, J.L., DeBeaumont, R., Saito, R.M., Hyberts, S.G., Yang, S., et al. (2006). An ARC/Mediator subunit required for SREBP control of cholesterol and lipid homeostasis. *Nature* **442**, 700–704.
- Zhang, C., Wendel, A.A., Keogh, M.R., Harris, T.E., Chen, J., and Coleman, R.A. (2012). Glycerolipid signals alter mTOR complex 2 (mTORC2) to diminish insulin signaling. *Proc. Natl. Acad. Sci. USA* **109**, 1667–1672.
- Zhang, Y., Zou, X., Ding, Y., Wang, H., Wu, X., and Liang, B. (2013). Comparative genomics and functional study of lipid metabolic genes in *Caenorhabditis elegans*. *BMC Genomics* **14**, 164.

Supplemental Information

Cholesterol-Independent SREBP-1 Maturation

Is Linked to ARF1 Inactivation

Lorissa J. Smulan, Wei Ding, Elizaveta Freinkman, Sharvari Gujja, Yvonne J.K. Edwards, and Amy K. Walker

Supplemental Figure legends and methods

Figure S1: In *C. elegans*, *lpin-1* and *arf-1.2* RNAi increase *pfat-7::GFP* expression in control, but not *sams-1(loid)* animals. Related to Figure 1. (A) Schematic diagram showing conversion of glycerol-3-phosphate to triglyceride and additional functions of enzymes acting in this pathway. Quantitative RT-PCR (qRT-PCR) comparing expression of endogenous stearoyl-CoA desaturases *fat-7*, *fat-5* and GFP after depletion of *lpin-1* and *arf-1.2* by RNAi in *pfat-7::GFP* (B) or *sams-1(loid);pfat-7::GFP* animals (C). Endogenous *fat-7* is increased in wild type animals in response to *lpin-1* or *arf-1.2* RNAi, however, it does not change with *plc-1* RNAi (D). (E) Quantitative RT-PCR (qRT-PCR) after depletion of *acl-4* and *acl-11* by RNAi in *pfat-7::GFP*. (F) Confocal projections show decreases in *pfat-7::GFP* after *acl-4* or *acl-11* RNAi. Confocal projection (G) or pixel intensity quantitation (H) of GFP::SBP-1 comparing nuclear and cytoplasmic levels after *acl-4* or *acl-11* RNAi. Error Bars show standard deviation. Results from student's T test shown by *p<0.05, **p<0.01, ***p<0.005.

Figure S2: The AGPATs *acl-4* and *acl-11* are important for *fat-7* expression and nuclear localization of GFP::SBP-1. Related to Figure 2. Confocal projections comparing GFP levels after RNAi of *acl-4* and *acl-11* in *pfat-7::GFP* (A) or *sams-1(loid);pfat-7::GFP* animals (C). Scale bar show 50 microns. Comparison of *fat-5*, *fat-7* and GFP expression by quantitative RT-PCR (qRT-PCR) after depletion of *acl-4* and *acl-11* by RNAi in *pfat-7::GFP* (B), *sams-*

1(loid);pfat-7::GFP animals (**D**) or *GFP::SBP-1* animals (**F**). Confocal projection (**E**) or pixel intensity quantitation (**G**) of *GFP::SBP-1* comparing nuclear and cytoplasmic levels after *acl-4* or *acl-11* RNAi. Scale bar shows 25 microns. Error Bars show standard deviation. Results from student's T test shown by *p<0.05, **p<0.01, ***p<0.005.

Figure S3: Lipidomic analysis of *C. elegans* microsomes. Related to **Figure 2.** (**A**) Fractionation of *C. elegans* extracts shows that Golgi or ER resident proteins are enriched in microsomal fractions. C is cytosolic, M is microsomal. Antibodies to SQV-8 and CYP-33E1 were developed and validated as part of the *C. elegans* Monoclonal antibody toolkit (Hadwiger et al., 2010) . CNX-1 is the ortholog of Calnexin. (**B**) Principal component analysis of lipidomic analysis of *C. elegans* cytosolic or microsomal extracts in control, *sams-1* or *lpin-1*(RNAi) animals. Closed circles represent microsomal and open/contrast colored show cytosolic extracts. Numbers represent biological replicates. (**C-G**) Comparison of lipid species from *C. elegans* microsomes shows distributions of lipid species within each class on a log scale. Solid lines show average for the class and each dot represents a recovered lipid species within the class. Because lipid species distribution was non-parametric, the Wilcoxon test was used for statistical significance (see also **Table S2** (then tab for lipid class), where these graphs are represented alongside relevant statistics). **** represents p values of <0.001. (**H, I**) Comparison of PA species in microsomal extracts from control, *sams-1* and *lpin-1*(RNAi) animals. (For individualized statistics, see also **Table S2; tab: PA**).

Error bars show standard deviation. Results from Paired T test shown by

*p<0.05, **p<0.01, ***p<0.005.

Figure S4: siRNA knockdown of *LPIN1* is similar to *PCYT1* depletion, increasing SREBP-1 nuclear accumulation in human hepatoma cells.

Related to **Figure 3**. Immunoblot of HA-SREBP-1 after siRNA of *PCYT1* (**A**) or *LPIN1* (**B**) from HepG2 cells. FL is the full-length cytoplasmic precursor and M is the mature nuclear version. (**C**) qRT-PCR demonstrating levels of *PCYT1* or *LPIN1* mRNA after siRNA knockdown. (**D**) Immunoblots of Dignam extracts after *PCYT1a* (PC) or *LPIN1* (LP) knockdown showing levels of Lipin 1 or CCTa in cytosolic or nuclear/ER extracts. Calnexin shows loading and histone 3 shows nuclear fraction. (**E**) Confocal projections of immunostaining comparing nuclear and cytoplasmic levels of endogenous SREBP-1 after combined knockdown of *PCYT1* or *LPIN1*. Quantitation of nuclear localization is shown in (**F**). Confocal projections (**G**), quantitation by lipid droplet (LD) area (**H**) or number (**I**) after Oil Red staining in HepG2 cells with *PCYT1*, *LPIN1* or combined siRNA. Graphs show combined data from three experimental sets. Results from student's T test shown by *p<0.05, **p<0.01, ***p<0.005 compared to scrambled (scr) conditions. Scale bars show 10 microns.

Figure S5: Localization and transcriptional activities of Lipin 1 are not changed by *PCYT1* siRNA.

Related to **Figure 3**. (A) Confocal projections of immunostaining to endogenous Lipin 1 in scrambled (scr) or *PCYT1* siRNA treated HepG2 cells with quantification of pixel intensity in (B). (C) Immunostaining of HepG2 cells for Lipin 1 after transfection with siRNA to scrambled (scr) controls or *LPIN1*. (D) Confocal projection of HepG2 cells transfected with a FLAG-LPIN1 construct and immunostained with anti-Flag antibodies. (E) Immunoblot of cells fractionated into Nuclear/ER, extracts (modified Dignam extract)(Andrews and Faller, 1991) probed with an antibody to Lipin 1. Histone 3 shows loading in nuclear fractions and Calnexin in fractions containing microsomes or ER. (F) qRT-PCR showing expression of β-oxidation gene mRNA after *PCYT1* siRNA. (G) Immunoblot of HepG2 cells transfected with siRNA to scrambled (scr), or *PCYT1a* and fractionated into microsomal or cytosolic fractions and probed with antibody to GBF1, ARFGAP1, and ARF1. β-actin shows loading and Calnexin in microsomal fractions. Results from student's T test shown by *p<0.05, **p<0.01, ***p<0.005. Error bars show standard deviation. Scale bars show 10 microns.

Table S1: *C. elegans* screen for low-PC modulators of SBP-1 activity.

Related to **Figure 1**. Screen table shows genes analyzed (Columns A,B), description (C) and functional category (D), chromosomal location (E), RNAi source (F), average of 4 scores from -3 (lowest) to +3 (highest) in screen for *pfat-7::GFP* (G) and *sams-1; pfat-7::GFP* (H). Scores below -0.75 are marked in blue and represent Class 1 for *pfat-7::GFP* or Class 3 for *sams-1(lof); pfat-7::GFP*. Scores above 0.75 are marked in yellow and show Class 2 for *pfat-7::GFP*.

Columns **I** and **J** show if growth was inhibited in the RNAi where as **K-M** note validation of selected RNAi results.

Table S2: Related to **Figure 2.** Lipidomic profiling of *C. elegans* microsomes after *sams-1* or *lpin-1* RNAi. **Table S2A:** Tabs in spread sheet show lipid classes with more than 10 species. Total class calculations are based on sums of all lipid species in class. **First tab (lipid):** Area normalized to total lipid for each lipid species in class. Averages for each row (species) along with standard deviations are shown along with fold changes of *sams-1* or *lpin-1* RNAi to control. Paired T Tests corresponding to data used for fold change calculations are also shown. All calculations were performed with Graphpad prism. **Second tab (lipid.class):** This tab contains details of the Wilcoxon test are also shown for *sams-1* or *lpin-1* RNAi vs control or *sams-1* vs *lpin-1* samples. A box and whisker plot is also shown. All calculations were performed with Graphpad Prism. Sum totals for the species in each class are included, with fold changes to controls and 3-tailed TTests.

Table S3: Related to **Figure 3.** Strains, siRNA constructs and antibodies.

Supplemental Methods:

C. elegans fractionation

Young adult *C. elegans* were collected, washed in s-basal buffer then pelleted animals were frozen in liquid N₂ and ground to a powder in a cold mortar (adapted from Kulas, et al). Next, the powder was resuspended in Tris Buffer I (50mM Tris, pH 7.5, 0.15M KCl, 0.25M sucrose, 2mM EDTA, 0.5mM DTT, 2.5 ug/ml ALLN, Complete protease inhibitor cocktail (Roche)) and gently homogenized with Dounce pestle B. Animals were further disrupted by bead-beating for 30 seconds for 5 intervals with one volume Ø 0.5 mm glass beads. Microsomes were purified by differential centrifugation (5 min at 3000g, 10 seconds at max in a microfuge at 4 °C, then 45 minutes at 80,000g) before resuspension of the pelleted microsomes in Tris-buffer II (50mM Tris pH 7.5, 20% glycerol, 5mM EDTA, 0.5 mM DTT, and Complete protease inhibitor cocktail (Roche)).

Lipidomics:

Lipid sample preparation

Chloroform was purchased from Sigma-Aldrich and was HPLC grade (ethanol-stabilized). Acetonitrile was purchased from EMD Millipore and was LC/MS Hypergrade. All other solvents were purchased from Fisher and were Optima LC/MS grade.

Cytosolic and microsomal samples (~250 uL and 50 uL, respectively) were supplemented with water up to a final volume of 300 ul, then mixed sequentially

with 600 uL methanol and 400 uL chloroform. After vortexing for 10 min. at 4°C, samples were centrifuged at 15,000xg for 10 min. at 4°C in a microcentrifuge. The bottom (lipid) fraction was collected and dried under vacuum. Dried lipid samples were typically dissolved in 50 ul 65:30:5 acetonitrile:isopropanol:water (v/v/v) and 5 ul was injected into the LC/MS, with separate injections for positive and negative ionization modes.

LC/MS experiments

Lipids were separated on an Ascentis Express C18 2.1 x 150 mm 2.7 µm column (Sigma-Aldrich, St. Louis, MO) connected to a Dionex UltiMate 3000 UPLC system and a QExactive benchtop orbitrap mass spectrometer (Thermo Fisher Scientific, San Jose, CA) equipped with a heated electrospray ionization (HESI) probe. Mobile phase A in the chromatographic method consisted of 60:40 water/acetonitrile in 10 mM ammonium formate (Sigma-Aldrich) and 0.1% formic acid (Pierce), and mobile phase B consisted of 90:10 isopropanol/acetonitrile, also with 10 mM ammonium formate and 0.1% formic acid. The chromatographic gradient was described previously (Hu et al., 2008). The column oven and autosampler tray were held at 55°C and 4°C, respectively. The MS instrument parameters were as described previously (Bird et al., 2011) and modified by (Ruzicka, J., McHale, K.J., and Peake, D.A. Data acquisition parameters optimization of quadrupole orbitrap for global lipidomics on LC-MS/MS time frame. Poster MP243 presented at 2014 American Society for Mass Spectrometry Annual Meeting, Baltimore, MD, June 15-20, 2014). The spray

voltage was set to 4.2 kV, and the heated capillary and the HESI were held at 320°C and 300°C, respectively. The S-lens RF level was set to 50, and the sheath and auxiliary gas were set to 35 and 3 units, respectively. These conditions were held constant for both positive and negative ionization mode acquisitions. External mass calibration was performed using the standard calibration mixture every 7 days.

MS spectra of lipids were acquired in full-scan / data-dependent MS² mode. For the full scan acquisition, the resolution was set to 70,000, the AGC target was 1e6, the maximum integration time was 50 msec, and the scan range was m/z = 133.4-2000. For data-dependent MS², the top 10 ions in each full scan were isolated with a 1.0 Da window, fragmented at a stepped normalized collision energy of 15, 25, and 35 units, and analyzed at a resolution of 17,500 with an AGC target of 2e5 and a maximum integration time of 100 msec. The underfill ratio was set to 0. The selection of the top 10 ions was subject to isotopic exclusion, a dynamic exclusion window of 5.0 sec, and an exclusion list of background ions based on a solvent blank.

Lipidomic data analysis

High-throughput identification and relative quantification of lipids was performed separately for positive and negative ionization mode data using LipidSearch software (Thermo Fisher Scientific / Mitsui Knowledge Industries) (Taguchi and Ishikawa, 2010; Yamada et al., 2013) using the default parameters for QExactive Product Search and Alignment. After alignment, raw peak areas

for all identified lipids were exported to Excel and filtered according to the following pre-determined quality control criteria: Rej ("Reject" parameter calculated by LipidSearch software) equal to 0; PQ ("Peak Quality" parameter calculated by LipidSearch software) greater than 0.85; CV (standard deviation / average peak area across triplicate injections of a representative [pooled] biological sample) below 0.4; R (linear correlation across a three-point dilution series of the representative [pooled] biological sample) greater than 0.9. Typically ~70% of identified lipids passed all four quality control criteria. Raw peak areas of the filtered lipids were added to generate a "total lipid signal" for each sample, and individual lipid peak areas were normalized to this total signal as a control for extraction efficiency and sample loading.

Bioinformatic analysis of lipiomic data:

PCA script is as follows:

```
countData <- read.table("pcalInput.txt",header=TRUE,row.names=1)
```

```
samples <- read.table("barcodes", header = TRUE, row.names =1)
```

```
dds <- DESeqDataSetFromMatrix(countData = countData,colData =  
samples,design = ~condition)
```

```
dds <- DESeq(dds)
```

```
dds <- dds[ rowSums(counts(dds)) > 1, ]
```

```
#pdf("plots2.pdf")
#select <-
order(rowMeans(counts(dds,normalized=TRUE)),decreasing=TRUE)[1:10]
hmcol <- colorRampPalette(brewer.pal(9, "GnBu"))(100)

# PCA
rld <- rlog(dds)
plotPCA(rld, intgroup=c("condition")) #title(main="PCAPlot",outer=TRUE)
```

Statistical analysis, including normality plots, significance tests by the Wilcoxon or paired T test methods were performed in GraphPad Prism following the methodology for statistical analysis of lipidomics samples outlined in (Checa et al., 2015).

Cell Fractionation II: HepG2 Dignam extracts

Transfected HepG2 cells were lysed and fractionated according to Andrews and Faller (1991). Briefly, transfected cell pellets were resuspended in ice cold Buffer A (10 mM Hepes-KOH, pH 7.9, 1.5 mM MgCl₂, 10 mM KCl, 1 mM DTT, 2.5 µg/mL ALLN, and protease inhibitor cocktail), then suspensions were incubated on ice for 10 min. Nuclei were isolated by centrifugation for 10 seconds, and resulting supernatant was centrifuged at 80,000 rpm for 45 min to isolate membrane fractions. The resulting supernatant was classified as the cytosolic fraction. Nuclear and membrane fractions were resuspended in ice cold buffer C (20 mM

Hepes-KOH, pH 7.9, 25% glycerol, 420 mM NaCl, 1.5 mM MgCl₂, 0.2 mM EDTA, 1 mM DTT, 2.5 µg/mL ALLN, and protease inhibitor cocktail).

Cell Fractionation III: HepG2 microsome

Transfected cell pellets were resuspended in ice cold Buffer A (10 mM Hepes-KOH, pH 7.9, 1.5 mM MgCl₂, 10 mM KCl, 1 mM DTT, 2.5 µg/mL ALLN, and protease inhibitor cocktail), then incubated on ice for 10 min. Nuclei were isolated by centrifugation for 10 seconds, and resulting supernatant was centrifuged at 80,000 rpm for 45 min to isolate microsome fraction with the supernatant reserved as the cytosolic fraction. Nuclear and microsome pellets were resuspended in ice cold buffer C (20 mM Hepes-KOH, pH 7.9, 25% glycerol, 420 mM NaCl, 1.5 mM MgCl₂, 0.2 mM EDTA, 1 mM DTT, 2.5 µg/mL ALLN, and protease inhibitor cocktail).

Supplemental References:

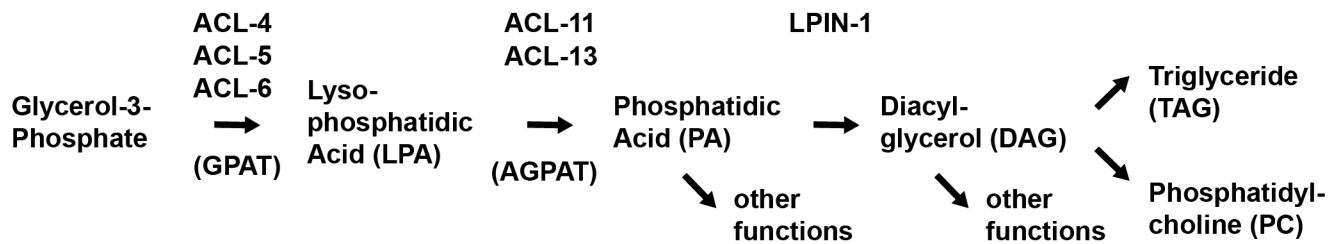
- Andrews, N.C., and Faller, D.V. (1991). A rapid micropreparation technique for extraction of DNA-binding proteins from limiting numbers of mammalian cells. *Nucleic Acids Res* 19, 2499.
- Bird, S.S., Marur, V.R., Sniatynski, M.J., Greenberg, H.K., and Kristal, B.S. (2011). Lipidomics profiling by high-resolution LC-MS and high-energy collisional dissociation fragmentation: focus on characterization of mitochondrial cardiolipins and monolysocardiolipins. *Anal Chem* 83, 940-949.
- Checa, A., Bedia, C., and Jaumot, J. (2015). Lipidomic data analysis: tutorial, practical guidelines and applications. *Analytica chimica acta* 885, 1-16.
- Hadwiger, G., Dour, S., Arur, S., Fox, P., and Nonet, M.L. (2010). A monoclonal antibody toolkit for *C. elegans*. *PloS one* 5, e10161.

Hu, C., van Dommelen, J., van der Heijden, R., Spijksma, G., Reijmers, T.H., Wang, M., Slee, E., Lu, X., Xu, G., van der Greef, J., *et al.* (2008). RPLC-ion-trap-FTMS method for lipid profiling of plasma: method validation and application to p53 mutant mouse model. *Journal of proteome research* 7, 4982-4991.

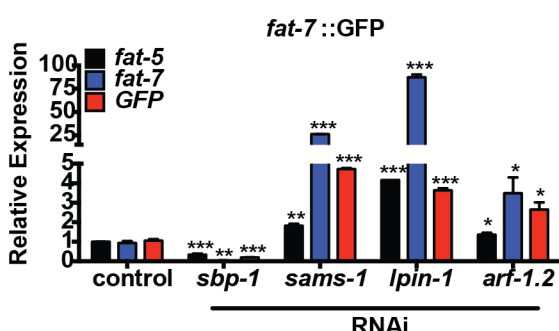
Taguchi, R., and Ishikawa, M. (2010). Precise and global identification of phospholipid molecular species by an Orbitrap mass spectrometer and automated search engine Lipid Search. *Journal of chromatography A* 1217, 4229-4239.

Yamada, T., Uchikata, T., Sakamoto, S., Yokoi, Y., Fukusaki, E., and Bamba, T. (2013). Development of a lipid profiling system using reverse-phase liquid chromatography coupled to high-resolution mass spectrometry with rapid polarity switching and an automated lipid identification software. *Journal of chromatography A* 1292, 211-218.

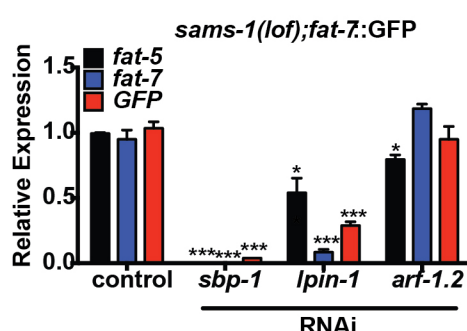
A



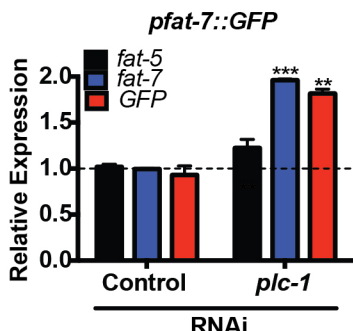
B



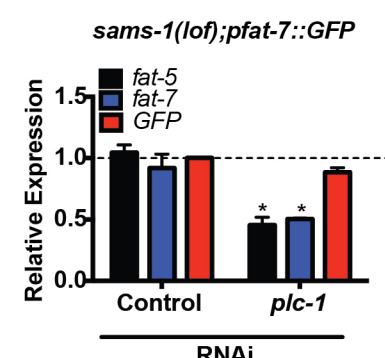
C



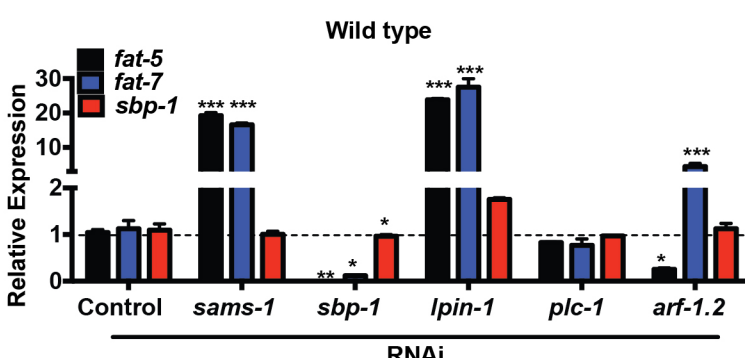
D



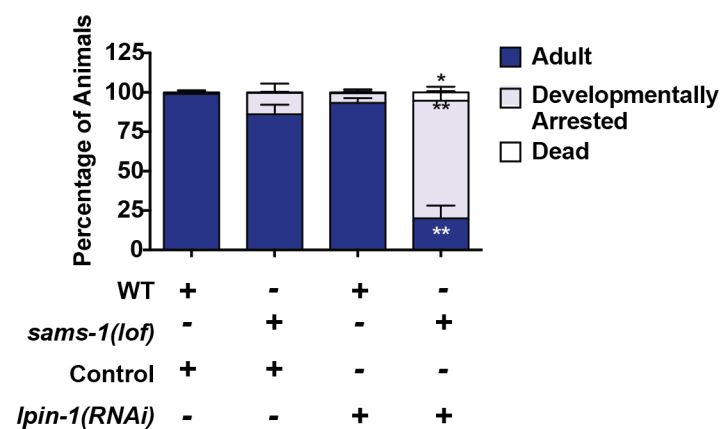
E



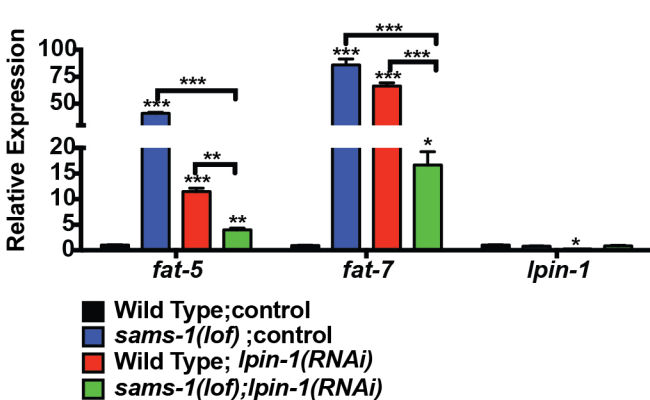
F



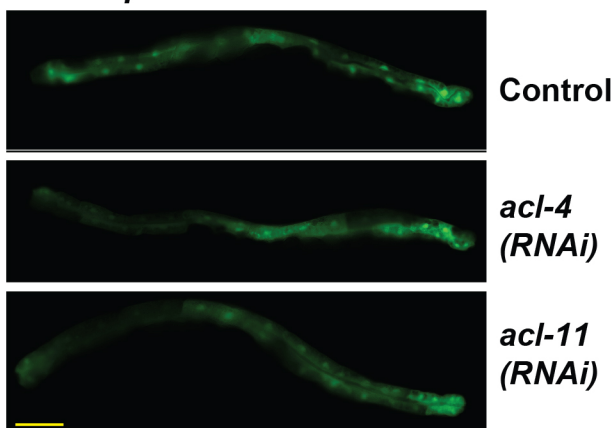
G



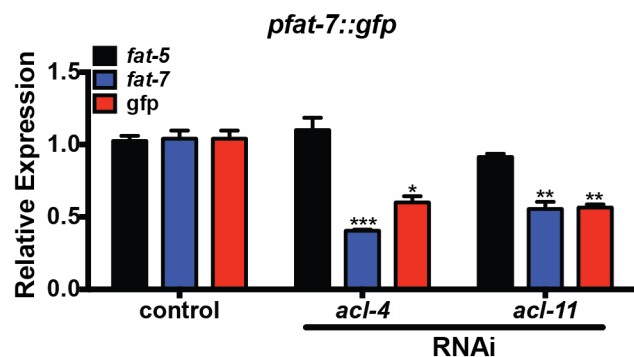
H



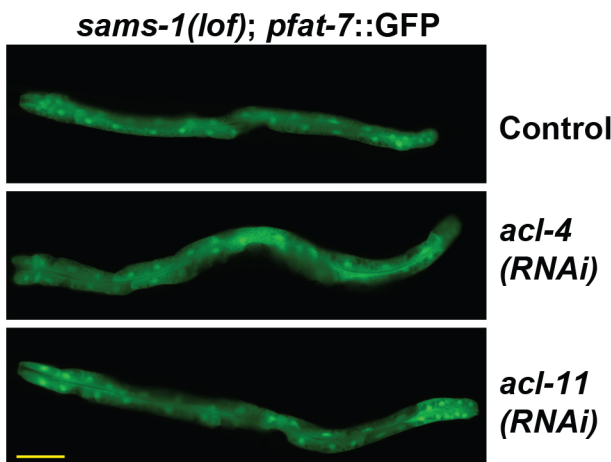
A *pfat-7::GFP*



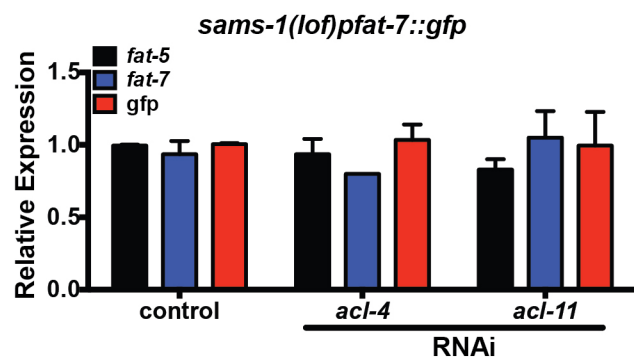
B



C

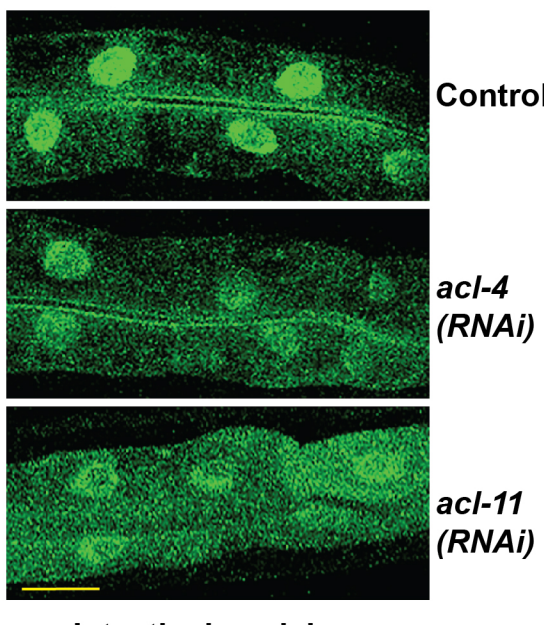


D

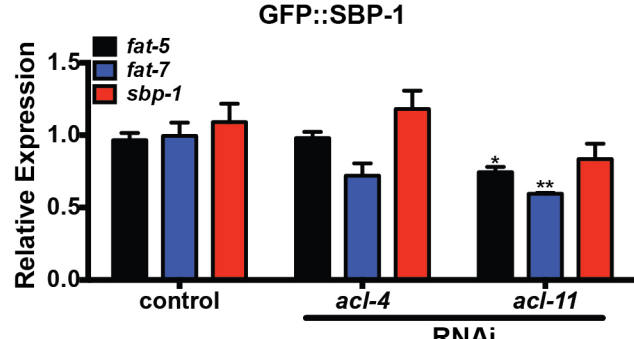


E

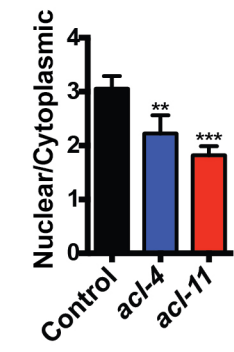
GFP::SBP-1



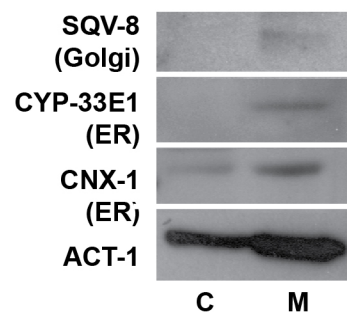
F



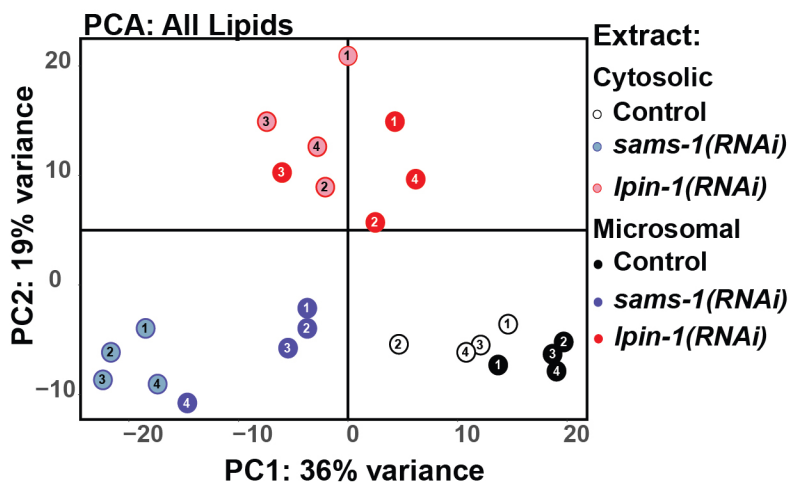
G



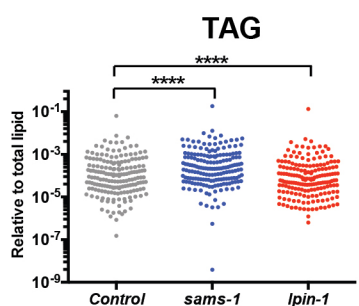
A



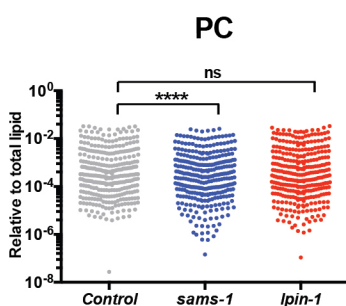
B



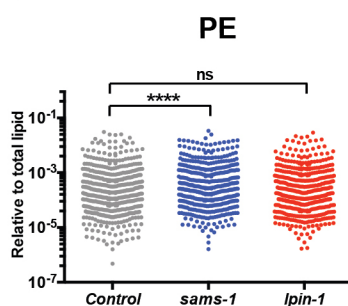
C



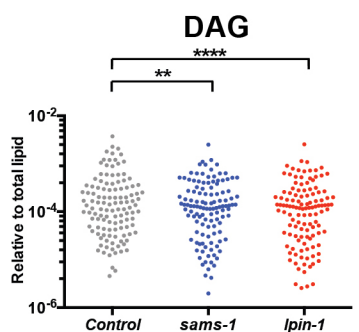
D



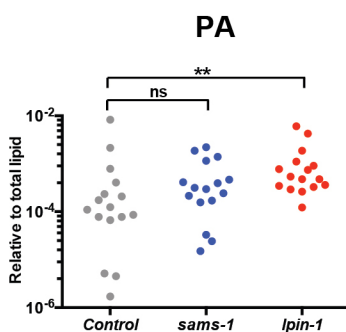
E



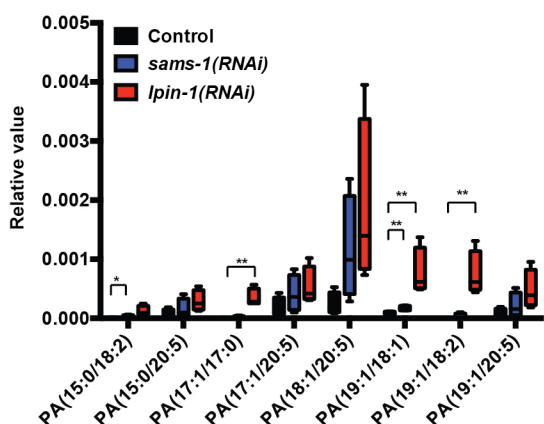
F



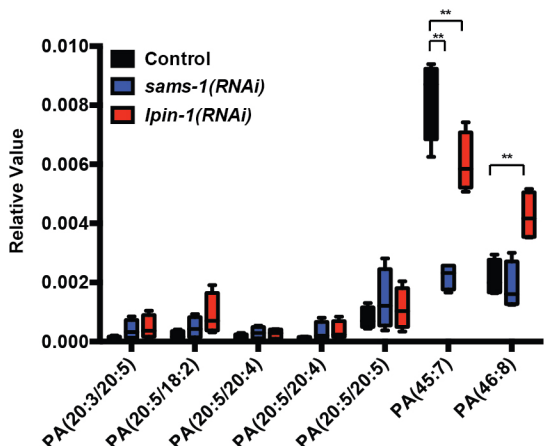
G



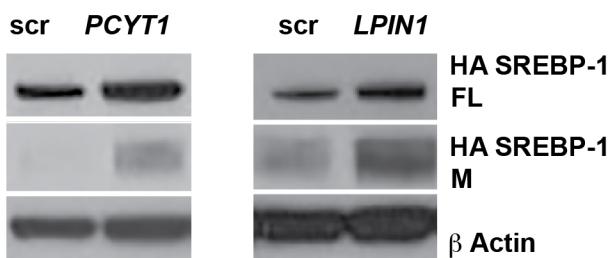
H



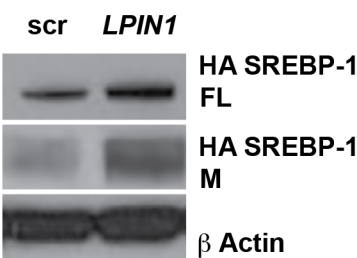
I



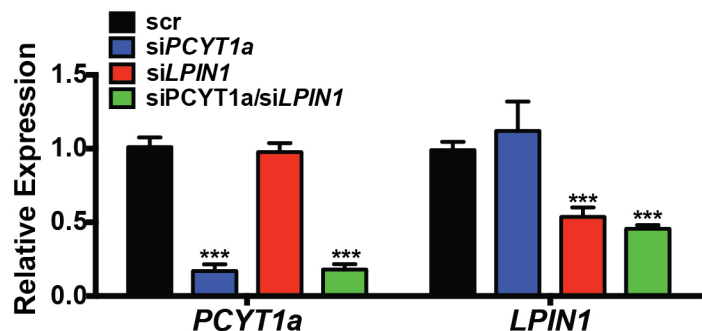
A



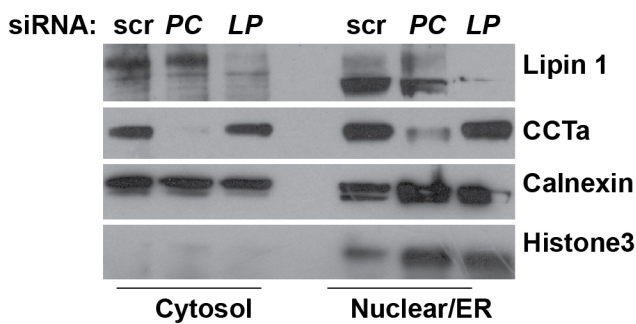
B



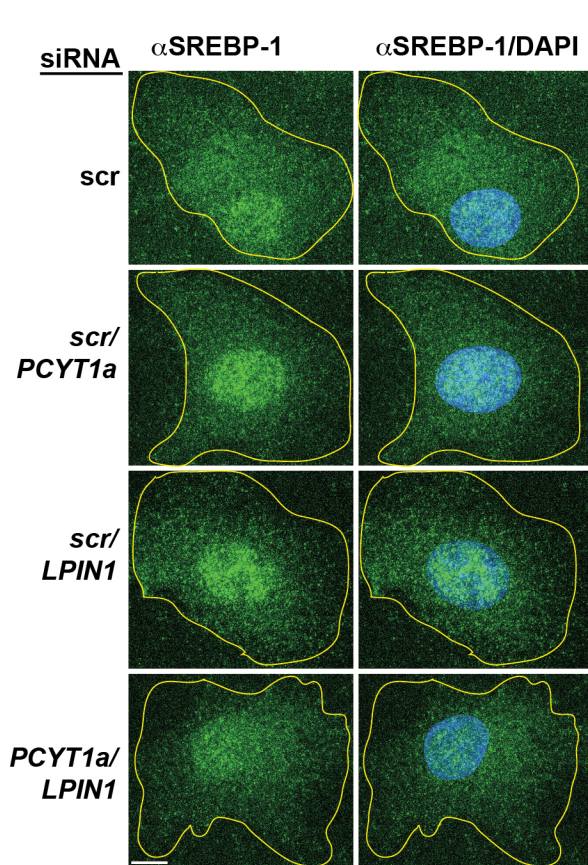
C



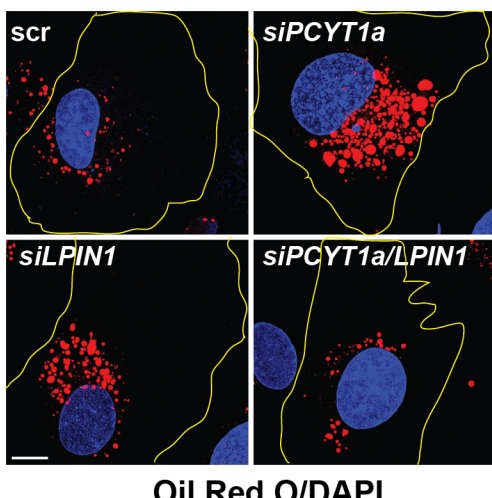
D



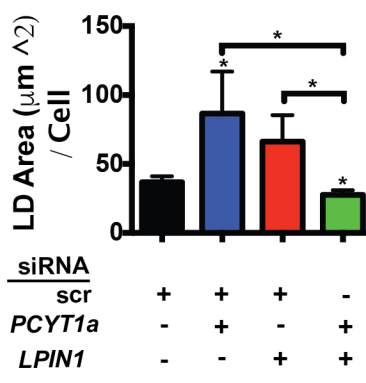
E



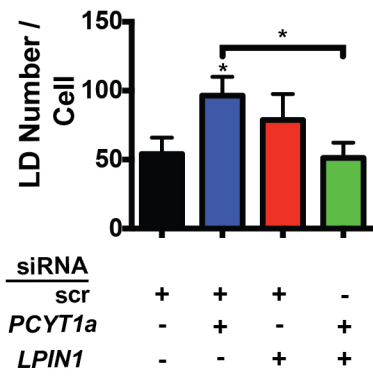
G



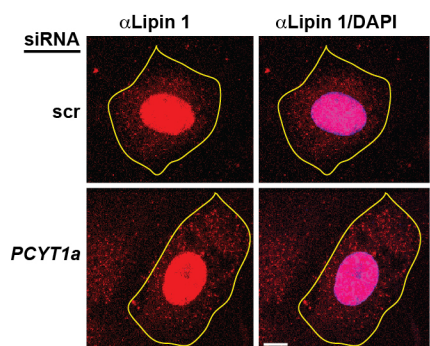
H



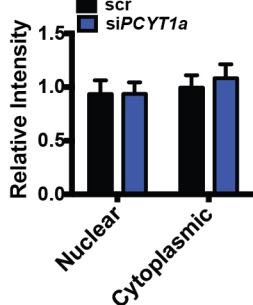
I



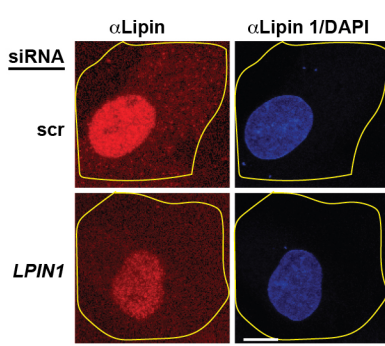
A



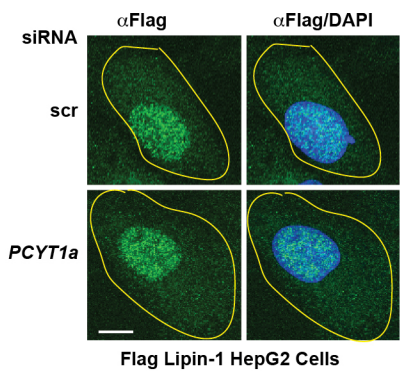
B



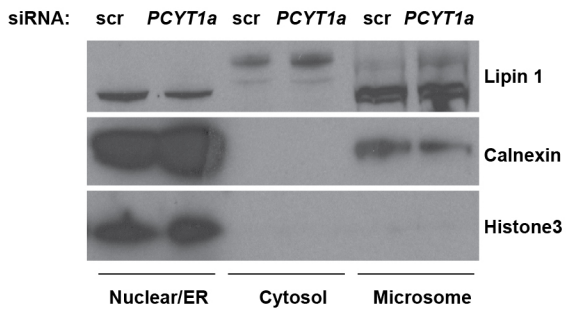
C



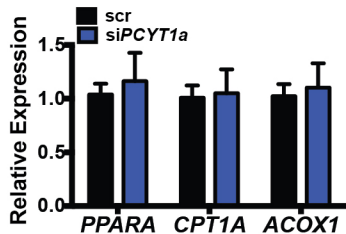
D



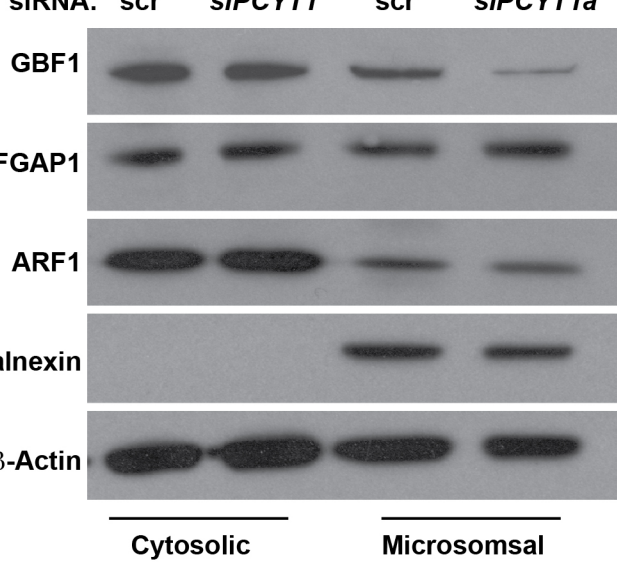
E



F



G



H

